Influence of inlet and bulk noise on Rayleigh-Bénard convection with lateral flow

D. Jung and M. Lücke

Institut für Theoretische Physik, Universität des Saarlandes, Postfach 151150, D-66041 Saarbrücken, Germany

A. Szprynger

Institute of Low Temperature and Structure Research, Polish Academy of Sciences, POB 1410, 50-950 Wrocław 2, Poland

Spatiotemporal properties of convective fluctuations and of their correlations are investigated theoretically in the vicinity of the threshold for onset of convection in the presence of a lateral through-flow using the full linearized equations of fluctuating hydrodynamics. The effect of external forcing by inlet boundary conditions on the downstream evolution of convective fields is separated from the effect of internal bulk thermal forcing with the use of spatial Laplace transformations. They show how the spatial variation of fluctuations and of their correlations are governed by the six spatial characteristic exponents of the field equations.

I. INTRODUCTION

The formation of macroscopic flow structures [1] in hydrodynamic systems like, e.g., Rayleigh-Bénard convection or Taylor-Couette flow that are driven out of thermal equilibrium by externally imposed heating or shear, respectively, are usually investigated by deterministic hydrodynamic field equations. However, under specific circumstances the influence of imperfections that break a symmetry of these equations, of external deterministic or stochastic perturbations, and of internal thermal noise on the pattern formation process should be taken into account to achieve a more realistic and quantitative description of experiments. One prominent example are the so-called noise sustained structures [2–12] in the convectively unstable parameter regime [13–15] in Taylor-Couette [4,5,8–10] and Rayleigh-Bénard [6,7,12] systems. They arise when an externally imposed through-flow or an internally generated group velocity is large enough to ''blow'' the pattern out of the system according to the deterministic hydrodynamic field equations. In this driving regime one observes in experiments [4,5,7,12] structures that are sustained by sources that generate perturbations in the band of modes that are amplified according to the supercritical deterministic growth dynamics in downstream direction sufficiently far away from the inlet. Another example are convective pattern fluctuations observed in closed containers in the subcritical driving range [16,17] where according to the deterministic equations the system would be quiescent.

Thermal-noise-generated fluctuating forces were introduced by Landau and Lifshitz [18] as volume coarse-grained microscopic fluctuations contributing to the stress tensor and the heat current. Then Zaitsev and Shliomis [19] and Graham [20] were the first to study the effect of this Gaussian additive white noise forcing on Rayleigh-Bénard convection [21]. A more general discussion of hydrodynamic field fluctuations out of equilibrium was given by Schmitz and Cohen for the Rayleigh-Bénard system [22]. Also the Ginzburg-Landau amplitude equation [1] describing slow spatiotemporal field variations in the vicinity of a pattern forming instability in terms of the amplitude of the critical mode has been

augmented by additive stochastic forcing [20,23,24,9,25]. Graham [20] used multiple scale expansion techniques to infer from the Landau-Lifshitz equations of fluctuating hydrodynamics the additive forcing entering into the amplitude equation. Schöpf and Zimmermann did the same for binary fluid mixtures [26]. Swift and Hohenberg used the critical behavior of correlation functions to find this relation for pure fluids in a simplified version without stochastic heat currents [23]. Boundary conditions for the amplitude equation in semi-infinite geometry were evaluated for a through-flow setup where microscopic transversal momentum density fluctuations are swept via the inlet into the bulk [8].

Besides the Ginzburg-Landau approximation the Swift-Hohenberg model equations [23] were used [24,27] with a stochastic forcing extension derived in Ref. [24] to compare with convection experiments in which the Rayleigh number was temporally ramped through threshold [28] or modulated periodically [29]. Also stochastic generalized Lorenz-like models obtained by truncating mode expansions of the hydrodynamic field equations were derived and compared [30] with the experiments [28,29]. The comparisons [24,27,30,31] of various model equations and in particular the work by van Beijeren and Cohen [32] incorporating the whole band of supercritically unstable modes showed that thermal noise was far too small to explain the experimental observations [28,29] with time-dependent heating quantitatively. However, the convective fluctuation intensity that was measured under static subcritical driving [17] was shown [17,33] to agree with the prediction [32] following from internal thermal noise based on linear fluctuating hydrodynamics. Recently experimental findings of subcritical fluctuating electroconvection in nematic crystals, i.e., a system with a much larger noise susceptibility than Rayleigh-Bénard convection were reported that showed deviations from linear fluctuating hydrodynamics [34].

The theoretical work done so far within the framework of the full fluctuating hydrodynamic field equations dealt with spatially extended systems making convenient use of spatial Fourier modes. However, in finite systems the effect of noise on pattern fluctuations—say, in the convectively unstable regime in downstream direction away from an inlet boundary—has been studied theoretically [2,3,6,8–11] only

by means of amplitude-equation approximations. A reason might be that the proper treatment, e.g., of the inlet boundary conditions for the fluctuating hydrodynamic field equations describing Rayleigh-Bénard convection with a lateral through-flow is somewhat intricate as shown in this work. Here we investigate within the full framework of linearized fluctuating hydrodynamics the effect of an externally imposed through-flow and the role that under such circumstances the inlet boundary conditions play in the downstream growth of convective fluctuations. Thus we distinguish between internal forcing due to thermal noise in our semi-infinite system and external forcing at the inlet, e.g., by perturbations that might enter the system via the through-flow.

A particular experimental Rayleigh-Bénard setup is possibly subject to other noise sources as well: For example, vibrations and rotations that accelerate the convection cell as a whole, thus exerting fluctuating (multiplicative) body forces; temperature fluctuations enforced from the outside on the boundaries of the cell, e.g., in the cooling and heating of the horizontal top and bottom plates, respectively; deformations of the cell caused by sound or by mechanical stresses that are generated by differentially moving fixtures. Compared to thermal-noise-generated fluctuations of the fluid itself (inside the cell or coming by the flow through the inlet into it) the above listed nongeneric perturbations can be controlled and diminished by appropriate experimental countermeasures. Moreover, in order for them to generate macroscopic flow structures in the convectively unstable regime they have to emit noise into the narrow band of modes that are amplified deterministically. So the noise would have to contain the right frequency in combination with the right wave number. Furthermore, among the noise sources that meet this requirement those that are operating close to or at the inlet are the most effective ones since they offer the longest amplification length/time for the noise-generated convective field perturbations to grow while being advected downstream.

Here we consider statistically stationary conditions when the inlet forcing and the thermal noise have been operating for a long time. In this situation we found it natural to Fourier decompose fields and forces in frequency space and then investigate the six characteristic complex spatial eigenvalues $K(\omega)$ of the hydrodynamic field equations that describe the spatial response to a perturbation of frequency ω and that govern the spatial variation of field fluctuations and their correlations. To evaluate them we use spatial Laplace transformations since this method allows for an easy separation of the effects of inlet forcing and bulk thermal forcing on fluctuating fields and on their correlation functions in a way that is similar to the treatment [11] of the amplitude equation in semi-infinite geometry.

The paper is organized as follows: In Sec. II we specify the system and the fluctuating hydrodynamic equations. In Sec. III we investigate its six spatial characteristic exponents and compare with the four exponents of the amplitude-equation approximation. In Sec. IV we briefly review the dynamics of fluctuations and correlations in infinite, translational invariant systems in comparison with the Ginzburg-Landau approximation before we elucidate in Sec. V the

fluctuation dynamics in semi-infinite systems. There we show how to separate bulk-generated fluctuation effects from inlet-generated fluctuations and how to evaluate correlation functions using spatial Laplace transforms. Section VI contains conclusions. Details on the treatment of inlet boundary conditions are given in Appendix A and Appendix B gives formulas for Laplace-transformed thermal force correlations.

II. SYSTEM

We consider a horizontal fluid layer of height d in the homogeneous gravitational field $\mathbf{g} = -g\,\mathbf{e_z}$ that is directed downwards. A positive temperature difference ΔT is imposed between the lower warm and upper cold confining boundaries. The associated Rayleigh number is

$$\mathrm{Ra} = \frac{\alpha g d^3}{\kappa \nu} \Delta T, \qquad (2.1)$$

where κ is the thermal diffusivity and ν the kinematic viscosity. The thermal expansion coefficient α follows from a linear isobaric equation of state for the mass density, $\rho/\rho_0 = 1 - \alpha(T - T_0)$, for small deviations of the temperature T from its mean T_0. We also consider a mean lateral through-flow $\bar{U}$ in x direction that is caused, e.g., by an externally applied pressure gradient with a through-flow Reynolds number $\mathrm{Re} = (d/\nu)\,\bar{U}$. We investigate here a small through-flow, say $\mathrm{Re} \leqslant 5$. In a layer of $d \simeq 0.5$ cm, $\nu \simeq 0.01$ cm^2/s (H_2O) the through-flow velocity for $\mathrm{Re} = 5$ would be $\bar{U} \simeq 0.1$ cm/s. Instead of Re we take the Péclet number

$$\mathrm{Pe} = \sigma\,\mathrm{Re} \qquad (2.2)$$

as second control parameter besides Ra. Here $\sigma = \nu/\kappa$ is the Prandtl number of the fluid.

A. Deterministic field equations

Ignoring thermal fluctuations the macroscopic behavior of the fluid is described by the balance equations for mass, momentum, and heat that we shall use in Oberbeck-Boussinesq approximation [18,35]

$$\boldsymbol{\nabla} \cdot \mathbf{U} = 0, \qquad (2.3a)$$

$$(\partial_t + \mathbf{U} \cdot \boldsymbol{\nabla})\mathbf{U} = \sigma \boldsymbol{\nabla}^2 \mathbf{U} - \boldsymbol{\nabla} P + \sigma(T - T_0)\mathbf{e_z}, \qquad (2.3b)$$

$$(\partial_t + \mathbf{U} \cdot \boldsymbol{\nabla})T = \boldsymbol{\nabla}^2 T. \qquad (2.3c)$$

Here $\mathbf{U} = U\mathbf{e_x} + V\mathbf{e_y} + W\mathbf{e_z}$ is the velocity field. We scale lengths with the height d of the fluid layer, time with the vertical thermal diffusion time d^2/κ, the effective pressure P with κ^2/d^2, and temperatures with $\kappa\nu/(\alpha g d^3)$.

1. Conductive state

For small Ra, Re a laterally homogeneous solution is stable that describes a so-called conductive state without vertical convective flow. In it the temperature

$$T_{cond} = T_0 + \text{Ra}\left(\frac{1}{2} - z\right) \qquad (2.4)$$

varies linearly between the temperatures

$$T(z=0) = T_0 + \frac{1}{2}\text{Ra}, \quad T(z=1) = T_0 - \frac{1}{2}\text{Ra}, \qquad (2.5)$$

that are imposed at the lower and upper boundaries, respectively. In addition there might be a lateral positive through-flow in x direction

$$\mathbf{U}_{cond} = U_{cond}\,\mathbf{e}_x. \qquad (2.6)$$

2. Horizontal boundary conditions

For no-slip horizontal boundaries with $\mathbf{U}=\mathbf{0}$ at $z=0$, 1 the through-flow is plane Poiseuille flow with parabolic velocity profile $U_{cond}^{ns} = 6\,\text{Pe}\,z\,(1-z)$. On the other hand, for free-slip impermeable horizontal boundaries that impose

$$W = \partial_z U = \partial_z V = 0 \quad \text{at } z=0,1, \qquad (2.7)$$

the through-flow has a z-independent plug flow profile, $U_{cond}^{fs} = \text{Pe}$. Such a through-flow can be transformed away by a Galilei transformation to a system that comoves with the plug-flow velocity if the fluid layer is laterally unbounded or if laterally periodic boundary conditions in x direction are applied.

In finite or semi-infinite geometry, however, where the externally imposed through-flow enters the system, say, at $x=0$ the effect of the through-flow on the convective perturbations that grow in downstream direction away from the inlet cannot be trivially transformed away. Since the no-slip Poiseuille through-flow yields in these laterally finite geometries similar effects on the downstream growing convection structures as in the analytically better manageable free-slip situation we shall investigate in this paper only the free-slip case (2.7).

B. Stochastic equations for deviations from the conductive state

The starting point for our investigation of the spatiotemporal behavior of the convective perturbations

$$\delta\mathbf{U} = \mathbf{U} - \mathbf{U}_{cond}, \quad \delta T = T - T_{cond}, \quad \delta P = P - P_{cond}, \qquad (2.8)$$

of the conductive state are the linearized field equations

$$\nabla \cdot \delta\mathbf{U} = 0, \qquad (2.9a)$$

$$(\partial_t + \text{Pe}\,\partial_x)\,\delta\mathbf{U} = -\nabla\,\delta P + \sigma\,(\nabla^2\,\delta\mathbf{U} + \delta T\,\mathbf{e_z}) + \mathbf{F}, \qquad (2.9b)$$

$$(\partial_t + \text{Pe}\,\partial_x)\,\delta T = \text{Ra}\,\delta W + \nabla^2\,\delta T + G, \qquad (2.9c)$$

for the fluctuations (2.8). They are generated by thermally fluctuating stresses $\sigma_{\alpha\beta}$ and heat currents $\mathbf{q}$ [18]

$$F_\alpha = \sum_{\beta=1}^{3} \nabla_\beta\,\sigma_{\alpha\beta}, \quad G = \nabla \cdot \mathbf{q}. \qquad (2.9d)$$

Here it is useful to consider $\mathbf{F} = \mathbf{F}_\perp + \mathbf{F}_\parallel$ to be decomposed into a "transversal" part that is divergence free, $\nabla \cdot \mathbf{F}_\perp = 0$, and into a "longitudinal" part without rotation, $\nabla \times \mathbf{F}_\parallel = 0$. The adjectives "transversal" and "longitudinal" refer to directions of $\mathbf{F}$ in wave-vector space. The longitudinal part $\mathbf{F}_\parallel$ forces "longitudinal" momentum, pressure, and mass density fluctuations (sound) that are decoupled from the "transversal" fluctuations of $\delta\mathbf{U}$ [18]. Since the longitudinal fluctuations of $\delta\mathbf{U}$ are not of interest for the growth of macroscopic convective structures we focus with Eq. (2.9a) on the transversal fluctuations. Then the pressure fluctuations are given according to Eq. (2.9) by

$$\nabla^2\,\delta P = \sigma\,\partial_z\,\delta T + \nabla \cdot \mathbf{F}. \qquad (2.10)$$

For the form of the stochastic forces $\mathbf{F}$ and G that enter into the equations (2.9) for the deviations from the conductive state we take as many previous authors the ansatz of Landau and Lifshitz [18], thus assuming local equilibrium to hold in the imposed vertical temperature gradient. Then the statistical properties of the real fluctuating forces are given by the following averages:

$$\langle F_\alpha(\mathbf{r},t)\rangle = \langle G(\mathbf{r},t)\rangle = \langle F_\alpha(\mathbf{r},t)\,G(\mathbf{r}',t')\rangle = 0, \qquad (2.11a)$$

$$\langle F_\alpha(\mathbf{r},t)\,F_\beta(\mathbf{r}',t')\rangle$$
$$= 2\,Q_2\left[\delta_{\alpha\beta}\,\nabla \cdot \nabla' + \nabla_\beta\nabla'_\alpha + \left(\frac{\zeta}{\nu\rho} - \frac{2}{3}\right)\nabla_\alpha\nabla'_\beta\right]$$
$$\times \delta(\mathbf{r}-\mathbf{r}')\,\delta(t-t'), \qquad (2.11b)$$

$$\langle G(\mathbf{r},t)\,G(\mathbf{r}',t')\rangle = 2\,Q_1\,\nabla \cdot \nabla'\,\delta(\mathbf{r}-\mathbf{r}')\,\delta(t-t'). \qquad (2.11c)$$

Since the temperature variation across the fluid layer is small when $\Delta T/T_0 \ll 1$ we use for the strength of the forces

$$Q_2 = k_B\,T_0\,\frac{\nu}{\rho\,d\,\kappa^3}, \quad Q_1 = \frac{T_0\,\alpha^2\,g^2\,d^4\,\kappa}{\nu^3\,c_p}\,Q_2, \qquad (2.12)$$

the equilibrium parameters evaluated at the mean temperature T_0 that appears in Eq. (2.12) in its unreduced form. Here c_p is the specific heat per unit mass and k_B is the Boltzmann constant.

A few remarks are in order: (i) In Eq. (2.11) lengths and times are reduced quantities. (ii) The volume viscosity ζ appears in Eq. (2.11b) in front of the "longitudinal" term $\sim \nabla_\alpha\nabla'_\beta$. It therefore does not enter into the correlations of the "transversal" velocity field fluctuations. (iii) Thermal heat current fluctuations are for most experimental setups much less relevant than stress fluctuations since, e.g., $Q_1/Q_2 \simeq 10^{-4}$ for a layer of water of height 1 cm at room temperatures. And finally, (iv) the spectral weight in frequency and wave-vector space of the stochastic forces (2.11) does not drop to zero for large ω and $\mathbf{k}$. This causes ultra-

violet divergence problems when evaluating in a direct way the mean square of velocity fluctuations resulting from Eq. (2.9) at a fixed $\mathbf{r},t$ via an integration over the whole frequency and wave-vector space. These convergence problems are due to extending the hydrodynamic theory (2.9) beyond its range of applicability to infinitely large wave vectors and frequencies. The problems do not arise when considering only the critical fluctuations, that have according to a linear deterministic theory the largest growth rates or smallest decay rates, respectively.

C. Projection onto critical modes

A standard-linear analysis [36] of the unforced dynamics of the convective perturbations (2.8) in laterally unbounded geometry gives an orthogonal basis of eigenmodes that spans the space of all solutions of Eqs. (2.9a–2.9c) with boundary conditions (2.5) and (2.7). It shows that modes of the form, e.g., $\delta T \sim \sin(\pi z)\, e^{ikx}\, e^{s(k)t}$ with wave number close to $k_c = \pi/\sqrt{2}$, no variation in y direction perpendicular to the direction of the wave vector $\mathbf{k}=k\mathbf{e_x}$, and a single maximum in vertical direction at mid height of the layer are the least damped. The characteristic exponent with the largest real part is

$$s(k) = -i\,k\,\mathrm{Pe} - \frac{\sigma+1}{2}\,q^2 + \sqrt{\left(\frac{\sigma-1}{2}\right)^2 q^4 + \sigma\,\mathrm{Ra}\,\frac{k^2}{q^2}},$$
$$(2.13)$$

where $q^2 = k^2 + \pi^2$. At the marginal stability boundary, $\mathrm{Ra}_{stab}(k) = q^6/k^2$, the growth rate $\mathrm{Re}\,s$ changes sign. The instability occurs for free-slip boundary conditions with the critical wave number $k_c = \pi/\sqrt{2}$ and critical frequency $\omega_c = k_c\mathrm{Pe}$ at $\mathrm{Ra}_c = 27\,\pi^4/4$. Modes with larger vertical variation, say $\sim \sin(2\pi z)$, can grow only at much higher Ra [36]. Therefore it suffices to consider here modes with the critical vertical profiles. For small $k - k_c$ and small

$$\epsilon = \frac{\mathrm{Ra}}{\mathrm{Ra}_c} - 1 \qquad (2.14)$$

the characteristic exponent (2.13) varies as

$$s(k) = -i k\,\mathrm{Pe} + [\epsilon - \xi_0^2\,(k-k_c)^2]/\tau_0, \qquad (2.15a)$$

and

$$\mathrm{Ra}_{stab}(k) = \mathrm{Ra}_c[1 + \xi_0^2(k-k_c)^2], \qquad (2.15b)$$

with

$$\xi_0^2 = \frac{8}{3\,\pi^2}, \qquad (2.16a)$$

$$\tau_0 = \frac{2}{3\,\pi^2}\,\frac{\sigma+1}{\sigma}. \qquad (2.16b)$$

In the remainder of this paper we project the fields (2.8) into the function subspace with the critical variation in z and

y. Thus, δW, δT, F_z, and G are projected in Eq. (2.9) onto $\sqrt{2}\,\sin(\pi z)$ while δU, δP, and F_x are projected onto $\sqrt{2}\,\cos(\pi z)$,

$$\begin{pmatrix} w \\ \theta \\ f_z \\ g \end{pmatrix}(x,t) = \frac{1}{\sqrt{2\,L_y}}\int_{-L_y}^{L_y} dy \int_0^1 dz\,\sqrt{2}\,\sin(\pi z)\begin{pmatrix} \delta W \\ \delta T \\ F_z \\ G \end{pmatrix}$$
$$\times (x,y,z,t), \qquad (2.17a)$$

$$\begin{pmatrix} u \\ p \\ f_x \end{pmatrix}(x,t) = \frac{1}{\sqrt{2\,L_y}}\int_{-L_y}^{L_y} dy \int_0^1 dz\,\sqrt{2}\,\cos(\pi z)\begin{pmatrix} \delta U \\ \delta P \\ F_x \end{pmatrix}$$
$$\times (x,y,z,t). \qquad (2.17b)$$

Here $2\,L_y$ is the "periodicity" length in y direction that we consider if necessary in the limit $L_y \to \infty$. Thus, we investigate convective perturbations with $k_y = 0$ that show no y variation. For such perturbations the dynamics of the velocity-field component in y direction, $\delta V(x,k_y=0,z,t)$, is decoupled from the other fields since $[\partial_t + \mathrm{Pe}\,\partial_x - \sigma\,(\partial_x^2 + \partial_z^2)]\,\delta V(x,k_y=0,z,t) = F_y(x,k_y=0,z,t)$. Hence we do not discuss δV fluctuations further.

We should like to mention that a convective channel with rectangular crosssection that is long in x direction and narrow in y direction, say of width $2L_y$ of the order of the layer height, is an appropriate experimental setup to enforce convective patterns of straight-parallel rolls with axes aligned in y direction and wave vector $\mathbf{k}=k_x\mathbf{e}_x$, i.e., $k_y=0$, also in the presence of a lateral through-flow. In that case the y projection in Eq. (2.17) would be on the critical y mode for this geometry. However, in systems where the width $2L_y$ is much larger than 1, experiments and numerical simulations of the hydrodynamic equations have shown [37–40] a competition between transverse rolls with axes perpendicular to the flow direction and longitudinal ones with roll axes aligned in flow direction that has also been investigated with coupled Ginzburg-Landau equations [41,42].

D. Projected field equations

The linear equations of motion for the fields (2.17) in the function subspace with the critical variation in z and y follow directly from Eq. (2.9). In view of the fact that a stochastic process described by Eqs. (2.9) and (2.11) is statistically stationary and since we are interested only in the long-time statistical dynamics of the fluctuations and not in their initial value dependence we found it most convenient to Fourier transform the fields (2.17) into frequency space, e.g., $w(x,\omega) = \int_{-\infty}^{\infty} dt\, e^{i\omega t}\, w(x,t)$. Henceforth we consider, unless otherwise stated, Fourier-transformed fluctuations depending on x and the real frequency ω. They obey the stochastic hydrodynamic equations (HE)

$$\partial_x u + \pi w = 0, \qquad (2.18a)$$

$$(-i\omega+\text{Pe}\,\partial_x)u=-\partial_x p+\sigma\,(\partial_x^2-\pi^2)\,u+f_x,$$
(2.18b)

$$(-i\omega+\text{Pe}\,\partial_x)w=\pi p+\sigma\,(\partial_x^2-\pi^2)\,w+\sigma\,\theta+f_z,$$
(2.18c)

$$(-i\omega+\text{Pe}\,\partial_x)\theta=(\partial_x^2-\pi^2)\,\theta+\text{Ra}\,w+g.$$
(2.18d)

The statistical behavior of the fluctuating forces projected according to Eq. (2.17) is given by

$$\langle f_\alpha(x,\omega)\rangle=\langle g(x,\omega)\rangle=\langle\,f_\alpha(x,\omega)[g(x',\omega')]^*\rangle=0,$$
(2.19a)

$$\langle f_\alpha(x,\omega)[f_\beta(x',\omega')]^*\rangle=2\,Q_2\,2\pi\delta(\omega-\omega')$$
$$\times S_{\alpha\beta}\,\delta(x-x'),\quad\text{(2.19b)}$$

$$\langle g(x,\omega)\,[g(x',\omega')]^*\,\rangle=2\,Q_1\,2\pi\delta(\omega-\omega')$$
$$\times(\partial_x\partial_{x'}+\pi^2)\,\delta(x-x'),$$
(2.19c)

with

$$S_{11}=\left(\frac{4}{3}+\frac{\zeta}{\nu\rho}\right)\partial_x\,\partial_{x'}+\pi^2,\quad S_{33}=\partial_x\,\partial_{x'}+\left(\frac{4}{3}+\frac{\zeta}{\nu\rho}\right)\pi^2,$$

$$S_{13}=\pi\left[\partial_{x'}-\left(\frac{\zeta}{\nu\rho}-\frac{2}{3}\right)\partial_x\right],\quad S_{31}=\pi\left[\partial_x-\left(\frac{\zeta}{\nu\rho}-\frac{2}{3}\right)\partial_{x'}\right].$$
(2.19d)

The superscript * in Eq. (2.19) and throughout this paper denotes complex conjugation. Here we have discarded any stress fluctuation σ_{13} at the horizontal boundaries $z=0,1$. So right at the horizontal boundaries thermal fluctuations do not change the lateral momentum balance of the fluid.

In order to investigate the spatial variations of the fluctuations of the fields u, w, θ, and p we also rewrite Eq. (2.18) into the system

$$(\mathcal{M}-\partial_x)\,\boldsymbol{\Psi}=\boldsymbol{\xi}$$
(2.20a)

of differential equations of first order in the x derivative for the six-component vectors

$$\boldsymbol{\Psi}=(\partial_x w,\partial_x\theta,p,u,w,\theta)^t,$$
(2.20b)

$$\boldsymbol{\xi}=\left(\frac{f_z}{\sigma},g,-f_x,0,0,0\right)^t$$
(2.20c)

of fields and forces, respectively, with

$$\mathcal{M}=\begin{pmatrix}\dfrac{\text{Pe}}{\sigma} & 0 & -\dfrac{\pi}{\sigma} & 0 & \pi^2-i\dfrac{\omega}{\sigma} & -1 \\[2mm] 0 & \text{Pe} & 0 & 0 & -\text{Ra} & \pi^2-i\omega \\[2mm] -\sigma\pi & 0 & 0 & i\omega-\sigma\pi^2 & \text{Pe}\,\pi & 0 \\[2mm] 0 & 0 & 0 & 0 & -\pi & 0 \\[2mm] 1 & 0 & 0 & 0 & 0 & 0 \\[2mm] 0 & 1 & 0 & 0 & 0 & 0\end{pmatrix}.$$
(2.20d)

The correlation matrix $\langle\xi_i(x,\omega)\,[\xi_j(x',\omega')]^*\rangle$ of the forces follows directly from Eq. (2.19).

E. GLE approximation

For Rayleigh numbers close to the critical one, i.e., for small ϵ the fluctuation dynamics around the heat-conductivity state can be described in form of a complex amplitude $A(x,t)$ multiplying the critical solution of the unforced equations (2.18) in time space

$$\begin{pmatrix}w(x,t)\\\theta(x,t)\end{pmatrix}=\begin{pmatrix}\hat{w}\\\hat{\theta}\end{pmatrix}A(x,t)\,e^{i(k_c x-\omega_c t)}+\text{c.c.},$$
(2.21)

where $\omega_c=k_c\,\text{Pe}$ and $\hat{w},\hat{\theta}$ are constants such that $\hat{\theta}/\hat{w}=\text{Ra}_c/q_c^2$. The amplitude obeys the stochastic Ginzburg-Landau equation (GLE) [20]

$$[\tau_0\,(\partial_t+v_g\,\partial_x)-\epsilon-\xi_0^2\,\partial_x^2]A(x,t)=\Gamma(x,t),\quad\text{(2.22)}$$

with a *complex* stochastic force $\Gamma(x,t)$. The statistical dynamics of Γ was derived [20,26] from Eq. (2.9) via a multiscale analysis to be of the form

$$\langle\Gamma(x,t)\rangle=\langle\,\Gamma(x,t)\,\Gamma(x',t')\rangle=0,$$
(2.23)

$$\langle\Gamma(x,t)\,[\Gamma(x',t')]^*\rangle=\gamma\,\delta(x-x')\,\delta(t-t').$$
(2.24)

In Sec. IV we will verify this result with

$$|\hat{w}|^2\gamma=\frac{4Q_2}{9\pi^2\sigma^2}\left(1+\frac{\sigma^2}{\text{Ra}_c}\frac{Q_1}{Q_2}\right),$$
(2.25)

with a different method that is more direct and less complicated than the standard-multiscale analysis.

Note that the coefficients c_0 and c_1 that normally appear in the complex GLE for oscillating patterns [1] vanish for the horizontal plug flow resulting from the free-slip boundary conditions. Furthermore, in this case one has

$$v_g = \text{Pe}. \qquad (2.26)$$

III. SPATIAL GROWTH BEHAVIOR

In Sec. II C we have reviewed the standard *temporal* growth analysis of a spatially extended mode $\sim e^{ikx}$ with real wave number k and laterally constant amplitude. Its relevant characteristic complex *temporal* exponent s Eq. (2.13) determines the oscillatory behavior and the exponential growth or decay behavior $e^{s(k)t}$ of this mode as a function of time t. Here we consider the *spatial* variation $e^{iK(\omega)x}$ of a "temporally extended" oscillatory mode $e^{-i\omega t}$, with real frequency ω and temporally constant amplitude that might be generated by a continuously operating spatially localized source of perturbation. The characteristic complex *spatial* exponent $K(\omega)$ determines via $\text{Re}\,K$ the wave number of the oscillatory mode and via $\text{Im}\,K$ its growth or decay with x.

A. Characteristic spatial exponents

The spatial variation in x direction of the field fluctuations in frequency space is governed by the six spatial characteristic exponents of Eq. (2.18) or, equivalently, of the 6×6 system of differential equations (2.20). In fact the solution of the deterministic equation (2.20a) with $\boldsymbol{\xi}=0$ is a superposition of the six eigenvectors $\boldsymbol{\Xi}_j$ ($j=1,2,\ldots,6$) of $\mathcal{M}$ multiplied by exponentials of the form

$$\boldsymbol{\Psi}_j = \boldsymbol{\Xi}_j\, e^{iK_j x}. \qquad (3.1)$$

Here iK_j is the jth eigenvalue of $\mathcal{M}$ and ω is the real frequency. The eigenvalues iK_j and eigenvectors $\boldsymbol{\Xi}_j$ depend on ω, Pe, and Ra. If necessary we denote the dependence on Ra also sometimes by the argument $\epsilon=\text{Ra}/\text{Ra}_c-1$.

In general the six eigenvalues K_j have to be calculated numerically. Being roots of the equation $\det(\mathcal{M}-iK)=0$ they, however, obey the relations

$$\sum_{j=1}^{6} K_j = -i\,\text{Pe}\left(1+\frac{1}{\sigma}\right), \qquad (3.2a)$$

$$\sum_{j=1}^{6} \frac{1}{K_j} = \text{Pe}\left(\frac{1}{\omega+i\,\pi^2}+\frac{1}{\omega+i\,\sigma\,\pi^2}\right), \qquad (3.2b)$$

$$\prod_{j=1}^{6} K_j = -\pi^2\,(\omega+i\,\pi^2)\left(\frac{\omega}{\sigma}+i\,\pi^2\right). \qquad (3.2c)$$

Furthermore, with $K_j(\omega,\text{Pe})$ also $-[K_j(-\omega,\text{Pe})]^* = K_l(\omega,\text{Pe})$ is one of the six eigenvalues and because of the mirror symmetry $-K_j(\omega,\text{Pe})=K_n(\omega,-\text{Pe})$. Moreover, the imaginary part of an eigenvalue $K_j(\omega,\text{Pe})$ can vanish only at the frequency $\omega_j^0=\text{Pe}\,\text{Re}\,K_j$ for our free-slip boundary conditions.
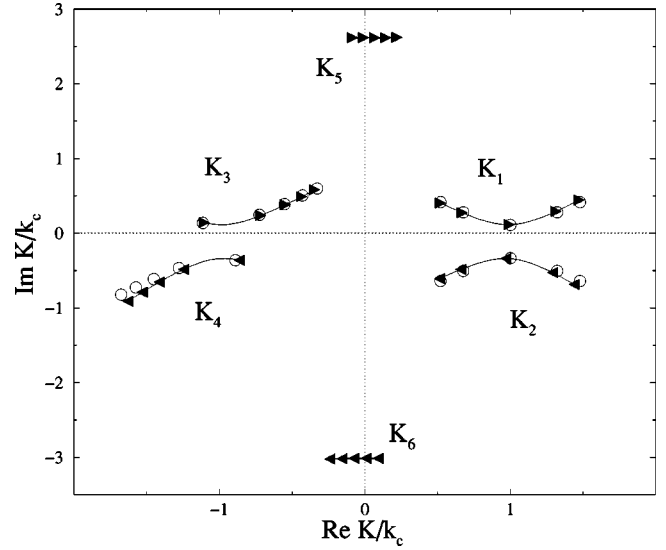

FIG. 1. Characteristic spatial exponents of the hydrodynamic equations (full arrows) and of the GLE approximation (open circles) in the complex wave-number plane. Orientations and locations of the arrows indicate how $K_j(\omega)$ varies with increasing frequency for $\omega-\omega_c=-5,-2,0,2,5$. The eigenvalues $K_{5,6}$ with the large imaginary parts do not appear by construction in the GLE. Parameters are $\sigma=1$, Pe$=1$, $\epsilon=-0.05$. With increasing ϵ, $K_1(K_3)$ crosses the real axis at $\epsilon=0$, k_c, ω_c ($-k_c$, $-\omega_c$). At the border ϵ_{conv}^c between convective and absolute instability the trajectories of K_1,K_2 and of K_3,K_4 touch, respectively. Beyond ϵ_{conv}^c they are reconnected differently.

In the following we consider the through-flow Péclet number to be positive. Then we chose the numbering of the six eigenvalues such that K_1 and K_3 are the two "critical" exponents that cross the real axis at $k=\pm k_c$ with critical frequency $\omega=\pm\omega_c=\pm\text{Pe}\,k_c$, respectively, when Ra $=\text{Ra}_c$. For the parameters investigated here the imaginary parts of the other eigenvalues remain finite. So we define K_5 to have positive imaginary part while those of K_2,K_4,K_6 are negative. The first four eigenvalues are pairwise related to each other by $K_3(\omega)=-[K_1(-\omega)]^*$ and $K_4(\omega) = -[K_2(-\omega)]^*$ while $K_5(\omega)=-[K_5(-\omega)]^*$ and $K_6(\omega) = -[K_6(-\omega)]^*$. Figure 1 shows the trajectories of all K_j for $\epsilon=-0.05$ in the complex wave-number plane as functions of ω.

The imaginary parts of $\{K_j\}$ determine the spatial growth or decay of a fluctuation with frequency ω while the real parts of $\{K_j\}$ denote its wave number. It should be noted that the characteristic spatial exponents—unlike the temporal exponent (2.13)—depend nontrivially on the through-flow that thus cannot be transformed away by a Galilei transformation. This shows already that a proper physical interpretation of the $\{K_j\}$ requires inhomogeneities or boundary conditions that break the translational invariance in the x direction. In this way one finds (cf. Sec. V) that the contributions $e^{iK_j x}$ with $j=2,4,6$ ($j=1,3,5$) to the fields $\boldsymbol{\Psi}$ describe the spatial variation in upstream (downstream) direction towards negative (positive) x resulting from a perturbation or from a boundary condition operating with frequency ω, say, at $x=0$. On the background of this identification one under-
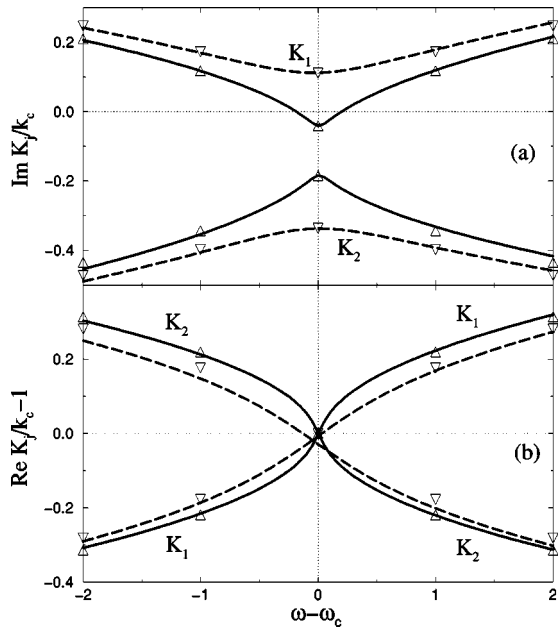
FIG. 2. Frequency dependence of the imaginary (a) and real (b) parts of the spatial eigenvalues K_1, K_2 of the hydrodynamic equations for subcritical driving $\epsilon = -0.05$ (dashed lines) and supercritical driving $\epsilon = 0.01$ (solid lines). The corresponding GLE approximation (3.7a) is shown by upwards (downwards) pointing triangles for $\epsilon = 0.01$ ($\epsilon = -0.05$). For the smallest $|\epsilon| = 0.01$ shown here only Im K_2 and Re K_1 display small deviations from their GLE behavior when ω differs sufficiently from ω_c. Parameters are $\sigma = 1$, Pe$=1$ so that $\epsilon = 0.01 < \epsilon^c_{conv}$.

stands quite naturally that the downstream-growth lengths $1/\text{Im}\, K_j$ ($j = 1,3,5$) increase with growing through-flow since the latter dilates the envelope of perturbations away from its source. On the other hand, the upstream-growth lengths $-1/\text{Im}\, K_j$ ($j = 2,4,6$) decrease with increasing Pe since the through-flow compresses the intensity envelope of the perturbations towards the source, making the growth steeper.

The fact that for positive ϵ the imaginary parts of the ''critical'' eigenvalues K_1 and K_3 are negative for bands of frequencies around $\pm \omega_c$, respectively, signals an instability via the downstream amplification of fluctuations with near critical frequencies. These bands open up at $\epsilon = 0$, $\omega = \pm \omega_c$ (cf. Fig. 2). The imaginary parts of the other characteristic exponents do not change sign with ϵ.

B. Spatial exponents of the GLE approximation

The GLE approximation ansatz (2.21) yields in ω space fields of the form, e.g.,

$$w(x,\omega) = \hat{w}\, e^{ik_c x} A(x, \omega - \omega_c) + [\hat{w}\, e^{ik_c x} A(x, -\omega - \omega_c)]^*. \tag{3.3}$$

The two spatial growth rates $\hat{K}_{1,2}$ of $A(x,\omega)$ defined by the two solutions of the unforced GLE (2.22) in frequency space of the form

$$A(x,\omega) \sim e^{i\hat{K}(\omega)x}, \tag{3.4}$$

are given by [11]

$$\hat{K}_{1,2}(\omega)\,\xi_0 = -i\,\sqrt{\epsilon^c_{conv}} \pm i\,\sqrt{\epsilon^c_{conv} - \epsilon - i\,\tau_0\,\omega}. \tag{3.5}$$

Here

$$\epsilon^c_{conv} = \frac{\tau_0^2}{4\,\xi_0^2}\, v_g^2 \tag{3.6}$$

is the boundary between convective and absolute instability within the GLE approximation [2]. Thus, the first two spatial exponents of $w(x,\omega)$ Eq. (3.3) are

$$K_{1,2}(\omega) = k_c + \hat{K}_{1,2}(\omega - \omega_c). \tag{3.7a}$$

They come from the first term in the GLE approximation (3.3). The next two exponents

$$K_{3,4}(\omega) = -k_c + \hat{K}_{1,2}(\omega + \omega_c), \tag{3.7b}$$

come from the second term in Eq. (3.3) where we have used the relation

$$\hat{K}_{1,2}(\omega) = -[\hat{K}_{1,2}(-\omega)]^* \tag{3.8}$$

or equivalently the relation $K_{1,2}(\omega) = -[K_{3,4}(-\omega)]^*$ that is discussed below Eqs. (3.2) to follow from the field equations.

Figures 1 and 2 show a comparison of the amplitude equation results (3.7) with the corresponding eigenvalues of the full-field equations. Note that within the GLE approximation the eigenvalues $K_{5,6}$ with the large imaginary parts implying small-scale variations do not appear since by construction the GLE is restricted to describe only slow-spatial variations. The agreement between the approximated and exact space eigenvalues $K_{1,\dots,4}$ improves with decreasing $|\epsilon|$ being the better the smaller Im K is.

Figure 2 shows the variation of imaginary part (a) and real part (b) of K_1 and K_2 with frequency ω for a subcritical $\epsilon = -0.05$ (dashed lines) and a supercritical $\epsilon = 0.01$ (full lines) below the threshold ϵ^c_{conv} in comparison with the GLE approximation (open triangles) discussed in Sec. III B.

C. Convective versus absolute instability

Whenever at a stability threshold the frequency of perturbations is nonzero with a finite group velocity $v_g = [\partial \omega(k)/\partial k]_c$, one has to distinguish between spatiotemporal growth behavior of spatially *extended* perturbations $\sim e^{\pm ik_c x}$ with real wave number $\pm k_c$ and of spatially *localized* or varying perturbations. The former have a positive *temporal* growth rate, Re $s(\pm k_c) > 0$, for Ra$>$Ra$_c$ according to Eq. (2.13). Equivalently the spatial growth exponents $K_{1,3}$ cross the real axis at $\pm(k_c, \omega_c)$ signalling for Ra$>$Ra$_c$ spatial growth for perturbations within a frequency band around $\pm \omega_c$ and a wave number band around $\pm k_c$. For the sake of notational conciseness we restrict our discussion to the case of K_1, k_c, ω_c. But the results apply as well to $K_3, -k_c, -\omega_c$.

Consider now a small spatially localized perturbation, i.e., a wave packet consisting of a linear superposition of extended perturbations of the form $\sim e^{ikx}$ with real k and small amplitude. For $Ra > Ra_c$ it might contain modes that can temporally grow, $Re\, s(k) > 0$, and others that decay. The center of such a wave packet or pulse perturbation propagates with the group velocity v_g while its envelope is growing since the pulse contains modes that grow in time.

Now there are two parameter regimes to be distinguished. (i) In the so called convectively unstable parameter regime [13–15] the wave packet moves with the velocity v_g faster away than it grows—while growing in the frame comoving with v_g the pulse moves out of the system so that the basic conductive state is restored in the absence of permanently operating forces. In other words, the two fronts that join the wave packet's intensity envelope to the structureless state propagate both in the direction in which the packet center moves. (ii) In the so called absolutely unstable parameter regime the growth rate of the packet is so large that one front propagates in the laboratory frame opposite to the center motion. Thus, the packet expands not only into the direction of the pulse motion but also opposite to it [13,14] so that eventually the initial perturbation can fill the entire system.

The boundary in parameter space between convective and absolute instability is marked by parameter combinations for which one of the fronts of the linear wave packet reverts its propagation direction in the laboratory frame: In the convectively unstable regime this front propagates in the same direction as the center of the packet, in the absolutely unstable regime it moves opposite to it, and right on the boundary between the two regimes the front is stationary in the laboratory frame. This parameter combination can be determined by a saddle-point analysis of the linear complex dispersion relation $s(K)$ over the plane of complex wave numbers [15].

The condition of vanishing front propagation velocity is equivalent to finding the parameters for which

$$Re\, s(K_*) = 0, \qquad (3.9a)$$

with K_* denoting the appropriate saddle position of $s(K)$ in the complex wave number plane given by

$$\left. \frac{ds(K)}{dK} \right|_{K_*} = 0. \qquad (3.9b)$$

The solution of Eq. (3.9) yields the sought-after boundary in parameter space between the convectively and the absolutely unstable parameter regime.

We have solved Eq. (3.9) numerically for the dispersion $s(K)$ Eq. (2.13) of the hydrodynamic field equations and compared the result for $\sigma = 1$ with the result of the GLE approximation. For the small Péclet numbers $Pe \lesssim 5$ explored here the saddle K_* of the HE dispersion relation (2.13) and the boundary $\epsilon^c_{conv}(Pe)$ of the HE agrees well with the GLE results $K_* = k_c - i(v_g \tau_0 / 2\xi_0^2) = k_c - (i/4)Pe$ and $\epsilon^c_{conv} = (\tau_0^2 / 4\xi_0^2)v_g^2 = (1/6\pi^2)Pe^2$, respectively. Note that $v_g = Pe$ and $c_1 = 0$ for the free-slip horizontal boundaries as mentioned earlier.

The conditions (3.9) for the boundary between convective and absolute instability imply the ''collision condition'' of Briggs [14],

$$\frac{d}{dK} \det[\mathcal{M}(\omega) - iK]\big|_{K_*} = 0, \qquad (3.10)$$

for the appearance of a double spatial eigenvalue. In Fig. 2 one sees how with increasing ϵ the two spatial eigenvalues K_1 (coming from the upper complex half plain) and K_2 approach each other. At $\epsilon = \epsilon^c_{conv}$ both branches meet at $K_1(\omega_*) = K_2(\omega_*) = K_*$. For our small Pe values ω_*^{HE} is very close to the GLE saddle frequency $\omega_*^{GLE} = \omega_c$.

For the driving $0 < \epsilon < \epsilon^c_{conv}$ a frequency band around ω_c with $Im\, K_1(\omega) < 0$ appears. Perturbations that are generated locally and sustained continuously with frequencies within this band are spatially amplified in downstream direction, i.e., in the direction of v_g. This frequency band is delimited within the GLE by $\omega_\pm = \omega_c \pm 2\sqrt{\epsilon \epsilon^c_{conv}}/\tau_0$ [8,11].

Note that our *linear* growth analysis of spatially varying perturbations is restricted to the driving range $\epsilon < \epsilon^c_{conv}$ where an initially localized perturbation is ''blown'' out of the system. In the driving range $\epsilon > \epsilon^c_{conv}$ of absolute instability, on the other hand, a perturbation acting with ω_* will grow at every location: the spatial eigenvalue $K_1(\omega_*)$ controlling the *linear* stationary solution $\sim e^{iK_1 x}$ loses its significance there since a *nonlinear* solution invades in upstream direction the whole system.

IV. LATERALLY UNRESTRICTED SYSTEMS

To better understand how a restricted geometry and inlet conditions, say at $x = 0$, influence the statistical dynamics of the fluctuating fields we first review the simpler case of a system that is extending from $x = -\infty$ to $x = \infty$.

A. Fluctuating hydrodynamics

In this section we discuss the statistical dynamics of the fluctuations of the convection fields $\Psi(x, \omega)$ Eq. (2.20b) that are produced by the thermally fluctuating forces $\xi(x, \omega)$ Eq. (2.20c).

In unrestricted geometry one can solve Eq. (2.20a) directly,

$$\Psi(k, \omega) = [\mathcal{M}(\omega) - ik]^{-1} \xi(k, \omega), \qquad (4.1)$$

via spatial Fourier transform $\Psi(k, \omega) = \int_{-\infty}^{\infty} dx\, e^{-ikx} \Psi(x, \omega)$ with k denoting a real wave number. In this way one finds

$$w(k, \omega) = \frac{\sigma k^2 g - ik\,(q^2 - i\Omega)\,(\pi f_x + ik f_z)}{D}, \qquad (4.2)$$

$$\theta(k, \omega) = \frac{(\sigma q^2 - i\Omega)\,q^2 g - ik\,Ra\,(\pi f_x + ik f_z)}{D}, \qquad (4.3)$$

with

$$D(k,\omega) = \sigma \, \det(\mathcal{M} - ik)$$

$$= q^2 \, (\sigma q^2 - i\Omega) \, (q^2 - i\Omega) - \sigma \, k^2 \, \mathrm{Ra}, \quad (4.4a)$$

$$\Omega = \omega - k \, \mathrm{Pe}, \quad q^2 = \pi^2 + k^2. \quad (4.4b)$$

The combination $\pi f_x + i k f_z$ of the forces is proportional to the z component of the ''transversal'' part $(\mathbf{f}_\perp)_z = (k/q^2)(\pi f_x + i k f_z)$. This reflects the fact that only ''transversal'' forces enter into the forcing of the ''transversal'' velocity field. The lateral velocity field fluctuations follow from Eq. (4.2) with the continuity equation $iku = -\pi w$ and pressure fluctuations follow directly from Eq. (2.10): $-q^2 p = \sigma \pi \theta + i k f_x + \pi f_z$. Thus we restrict our discussion to w and θ only.

Note that the fluctuations with the critical wave numbers and frequencies $\pm(k_c, \omega_c)$ are strongly amplified when Ra is increased. They diverge at Ra_c with, e.g.,

$$D(k_c, \omega_c) = (\mathrm{Ra}_c - \mathrm{Ra}) \, \sigma \, k_c^2 \quad (4.5)$$

vanishing linearly. It is obvious from Eqs. (4.2) and (4.3) that the characteristic determinant $D(k,\omega)$ Eq. (4.4) of the deterministic hydrodynamic field equations governs the $\omega-k$ dependence of the instability-driven amplification mechanism.

From Eqs. (4.2) and (4.3) and using Eq. (2.19) one directly obtains the correlation functions

$$C_{ww}(k,\omega) = \frac{\langle \, w(k,\omega) \, [w(k',\omega')]^* \rangle}{(2\pi)^2 \, \delta(\omega - \omega') \, \delta(k - k')} \quad (4.6a)$$

$$= 2Q_2 \, \frac{k^2 q^4 \, (\Omega^2 + q^4)}{|D|^2}$$

$$\times \left(1 + \frac{Q_1}{Q_2} \frac{k^2}{q^2} \frac{\sigma^2}{\Omega^2 + q^4} \right), \quad (4.6b)$$

$$C_{\theta\theta}(k,\omega) = 2Q_2 \, \mathrm{Ra}^2 \, \frac{k^2 q^4}{|D|^2} \left[1 + \frac{Q_1}{Q_2} \frac{q^2}{k^2} (\Omega^2 + \sigma^2 q^4) \right]. \quad (4.7)$$

Here we used the fact that with $\boldsymbol{\xi}(x,t)$ being real one has $[\boldsymbol{\xi}(k,\omega)]^* = \boldsymbol{\xi}(-k,-\omega)$. The same holds for w and θ.

Note that because of Eq. (4.5) the correlation functions of the critical modes $\pm(k_c, \omega_c)$ diverge $\sim 1/\epsilon^2$ for $\epsilon \to 0^-$ within the linear theory of fluctuating hydrodynamics. Since here the fluctuations are spatially extended $\sim e^{ikx}$ with real wave number k there does not appear by construction a supercritical driving range where convectively unstable perturbations could be blown out of the system. Such a situation can arise only in restricted geometry with spatially varying amplitudes. Thus, here in Sec. IV the linear analysis of extended modes with wave number k is restricted to the driving range $\mathrm{Ra} < \mathrm{Ra}_{stab}(k)$.

B. Fluctuating hydrodynamics versus GLE approximation

The statistical dynamics of the fluctuating fields within the GLE approximation is readily obtained from solving the amplitude equation (2.22) by double Fourier transform

$$A(k,\omega) = \frac{-\Gamma(k,\omega)}{\epsilon - \xi_0^2 k^2 + i(\omega - k \, v_g) \, \tau_0}, \quad (4.8)$$

and using the field representation (2.21) leading to

$$\begin{pmatrix} w(k,\omega) \\ \theta(k,\omega) \end{pmatrix} = \begin{pmatrix} \hat{w} \\ \hat{\theta} \end{pmatrix} A(k - k_c, \, \omega - \omega_c)$$

$$+ \begin{pmatrix} \hat{w} \\ \hat{\theta} \end{pmatrix}^* [A(-k - k_c, \, -\omega - \omega_c)]^*. \quad (4.9)$$

Here $\omega_c = k_c v_g = k_c \, \mathrm{Pe}$. Since

$$\langle \Gamma(k,\omega) \, [\Gamma(k',\omega')]^* \rangle = \gamma(2\pi)^2 \, \delta(k - k') \, \delta(\omega - \omega'), \quad (4.10)$$

one immediately obtains that within the GLE approximations (4.8) and (4.9) the field correlations are given by

$$C_{ww}^{GLE}(k,\omega) = |\hat{w}|^2 \, \gamma \left\{ \frac{1}{[\epsilon - \xi_0^2 \, (k - k_c)^2]^2 + (\omega - k \, v_g)^2 \, \tau_0^2} \right.$$

$$\left. + \frac{1}{[\epsilon - \xi_0^2 \, (k + k_c)^2]^2 + (\omega - k \, v_g)^2 \, \tau_0^2} \right\}, \quad (4.11a)$$

$$C_{\theta\theta}^{GLE}(k,\omega) = \frac{|\hat{\theta}|^2}{|\hat{w}|^2} \, C_{ww}^{GLE}(k,\omega), \quad (4.11b)$$

with $\hat{\theta}/\hat{w} = \mathrm{Ra}_c/q_c^2$. Here we have used the fact that the vanishing of $\langle \Gamma(k,\omega)\Gamma(k',\omega') \rangle$ that follows from Eq. (2.23) implies $\langle A(k,\omega)A(k',\omega') \rangle = 0$ as well whereas

$$\langle A(k,\omega) \, [A(k',\omega')]^* \rangle = \gamma \frac{(2\pi)^2 \, \delta(k - k') \, \delta(\omega - \omega')}{(\epsilon - \xi_0^2 k^2)^2 + (\omega - k \, v_g)^2 \, \tau_0^2}. \quad (4.12)$$

1. Identification of γ

One can elegantly and conveniently determine the forcing strength γ in the stochastically forced GLE (2.22) without having to go to the lengthy multiple-scale derivation of Ref. [20]. To that end we require that the fluctuation spectra (4.11) obtained within the GLE approximation agree with the hydrodynamic fluctuation spectra (4.6) and (4.7) based on the full-field equations for the critical fluctuations with wave number k_c and frequency ω_c when approaching the pattern forming instability threshold of the unforced field equations,

i.e., in the limit $\epsilon \to 0^-$. Thus identifying the divergence $\sim (1/\epsilon^2)$ of Eq. (4.6) for k_c, ω_c and $\epsilon \to 0$ with the same one of Eq. (4.12) one finds

$$|\hat{w}|^2 \gamma = 2 Q_2 \frac{q_c^2}{\sigma^2 \mathrm{Ra}_c} \left(1 + \frac{Q_1}{Q_2} \frac{\sigma^2}{\mathrm{Ra}_c} \right), \qquad (4.13)$$

and similarly

$$|\hat{\theta}|^2 \gamma = 2 Q_2 \frac{\mathrm{Ra}_c}{\sigma^2 q_c^2} \left(1 + \frac{Q_1}{Q_2} \frac{\sigma^2}{\mathrm{Ra}_c} \right). \qquad (4.14)$$

Swift and Hohenberg [23] have identified γ in a somewhat similar approach neglecting, however, the small contribution $\sim Q_1$. Our result (4.13) and (4.14) agrees with the result obtained in [26] when one uses as in [26] the scaling of the critical modes in which $\hat{w} = 1$ and $\hat{\theta} = \mathrm{Ra}_c/q_c^2$. For a direct comparison one has to note that these authors have evaluated γ for a two-component mixture. Therefore, one has to set in Eq. (5.12) of Ref. [26] the separation ratio $\Psi = 0$ that corresponds to our case of a one-component fluid. The same result was obtained also by Graham [20].

2. Comparison of the spectra $C(k,\omega)$

Figure 3 shows that the GLE approximation,

$$C_{ww}^{GLE}(k,\omega) = 2 Q_2 \frac{q_c^2}{\sigma^2 \mathrm{Ra}_c} \left(1 + \frac{Q_1}{Q_2} \frac{\sigma^2}{\mathrm{Ra}_c} \right)$$

$$\times \left\{ \frac{1}{[\epsilon - \xi_0^2 (k - k_c)^2]^2 + (\omega - k\,v_g)^2\,\tau_0^2} \right.$$

$$\left. + \frac{1}{[\epsilon - \xi_0^2 (k + k_c)^2]^2 + (\omega - k\,v_g)^2\,\tau_0^2} \right\},$$

$$(4.15)$$

$$C_{\theta\theta}^{GLE}(k,\omega) = \frac{\mathrm{Ra}_c^2}{q_c^4} C_{ww}^{GLE}(k,\omega), \qquad (4.16)$$

agrees quite well with the fluctuation spectra $C_{ww}(k,\omega)$ Eq. (4.6) and $C_{\theta\theta}(k,\omega)$ Eq. (4.7), respectively, for the small values of $\epsilon = -0.05$ and $\epsilon = -0.1$ shown there. The left column shows $C(k_c,\omega)$ versus ω and the right column $C(k,\omega_c)$ versus k both for Pe=5. In each case we have ignored the small contributions $\sim Q_1/Q_2$ in Eqs. (4.6) and (4.7) and in Eqs. (4.15) and (4.16).

Here and in the following the GLE result for w fluctuations agrees better with the spectrum of fluctuating hydrodynamics than the spectrum of θ fluctuations. The reason lies in the ratio

$$\frac{C_{\theta\theta}(k,\omega)}{C_{ww}(k,\omega)} = \frac{\mathrm{Ra}^2}{\Omega^2 + q^4} \qquad (4.17)$$
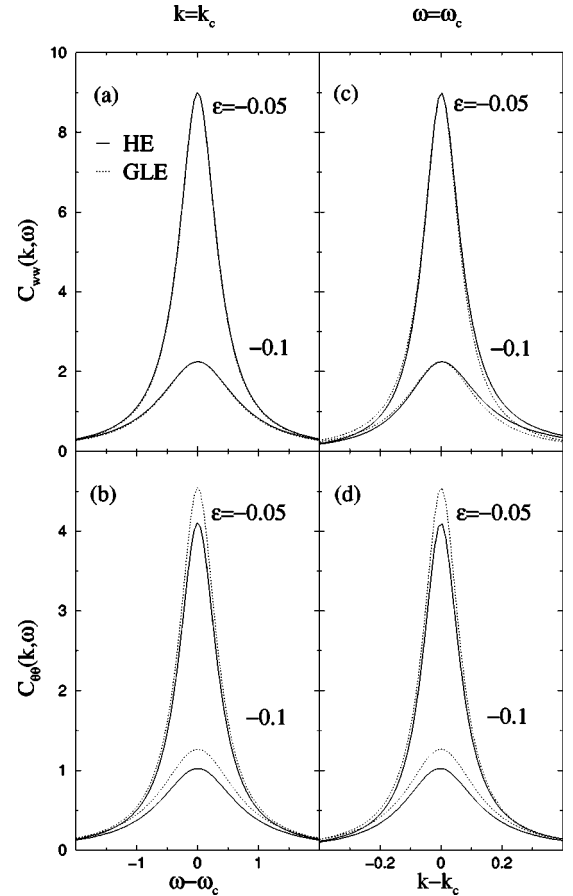

FIG. 3. Reduced correlation spectra of vertical velocity fluctuations (a,c) and of temperature fluctuations (b,d) resulting in a laterally infinite system from fluctuating hydrodynamics (full lines) and from the GLE approximation (dotted lines). The left column (a,b) shows frequency spectra for $k = k_c$ and the right column (c,d) wave-number spectra for $\omega = \omega_c$. The spectra diverge with increasing ϵ at $\epsilon = 0, k_c, \omega_c$ as discussed in the text. Parameters are $\sigma = 1$, Pe=5. $C_{ww}(C_{\theta\theta})$ is reduced by $2 Q_2$ (0.02 Q_2 Ra^2).

depending on k, ω, Ra, and Pe while the GLE yields for this ratio of mean square amplitude fluctuations the constant Ra_c^2/q_c^4.

3. $C(x=0,\omega)$

In Fig. 4 we compare the frequency dependence of the total spectral weight in wave-number space

$$C(x=0,\omega) = \int_{-\infty}^{\infty} \frac{dk}{2\pi} C(k,\omega) \qquad (4.18)$$

for w and θ fluctuations that result from fluctuating hydrodynamics with those following from the GLE approximation

$$C_{ww}^{GLE}(x=0,\omega) = Q_2 \frac{q_c^2}{\xi_0^4 \sigma^2 \mathrm{Ra}_c} \left(1 + \frac{Q_1}{Q_2} \frac{\sigma^2}{\mathrm{Ra}_c} \right)$$

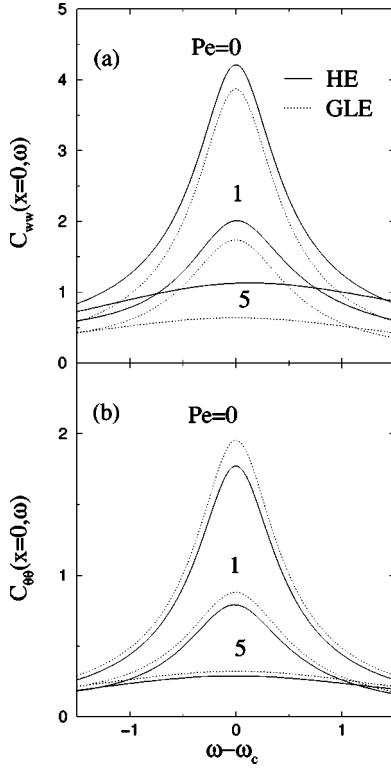$$\times [G(\omega - \omega_c) + G(\omega + \omega_c)], \qquad (4.19a)$$

FIG. 4. Frequency dependence of the reduced total spectral weight in wave-number space, $C(x=0,\omega)$, of velocity fluctuations (a) and of temperature fluctuations (b) according to the hydrodynamic equations (full lines) in comparison with the GLE approximation (dotted lines) for different through-flow Péclean numbers as indicated. Parameters are $\sigma=1$, $\epsilon=-0.05$. $C_{ww}(C_{\theta\theta})$ is reduced by $2Q_2$ $(0.02\ Q_2\ \mathrm{Ra}^2)$.

$$C_{\theta\theta}^{GLE}(x=0,\omega)=\frac{\mathrm{Ra}_c^2}{q_c^4}\,C_{ww}^{GLE}(x=0,\omega). \qquad (4.19b)$$

In the first (second) contribution of

$$G=\frac{1}{|\hat{K}_1-\hat{K}_2|^2}\left(\frac{1}{\mathrm{Im}\,\hat{K}_1}-\frac{1}{\mathrm{Im}\,\hat{K}_2}\right) \qquad (4.19c)$$

in the square bracket of Eq. (4.19a) the arguments of the GLE approximation (3.5) for $\hat{K}_{1,2}$ are $\omega-\omega_c$ $(\omega+\omega_c)$. Unfortunately the complexity of the hydrodynamic spectra does not allow for an analytical wave-number integration of Eqs. (4.6) and (4.7).

With increasing through-flow the fluctuation intensity $C(x=0,\omega)$ decreases for frequencies close to ω_c and spreads over a broader band around ω_c. The time-displaced correlations of fluctuations at the common position are reduced since in a finite through-flow fluctuations that are generated also by forces operating further away in upstream direction enter into the correlator. The difference between the hydrodynamic fluctuation strength $C_{ww}(x=0,\omega)$ and the GLE approximation $C_{ww}^{GLE}(x=0,\omega)$ grows since the hydrodynamic velocity field fluctuations are enhanced by the factor $(\Omega^2 +q^4)$ in the numerator of Eq. (4.6b)—the growth in Pe leads

via $\Omega^2=(\omega-k\,\mathrm{Pe})^2$ to an increased weight of the large-k modes for which the GLE approximation deteriorates.

4. $C(k,t=0)$

Finally, we discuss the wave-number dependence of the total spectral weight

$$C(k,t=0)=\int_{-\infty}^{\infty}\frac{d\omega}{2\pi}C(k,\omega) \qquad (4.20)$$

in frequency space. This mean-squared amplitude of a k mode is for free-slip horizontal boundaries independent of the through-flow—the Pe dependence drops out in integrations over all ω reflecting the invariance of the laterally unbounded system with free-slip horizontal boundaries and plug flow under a Galilean transformation. One finds

$$C_{ww}(k,t=0)=\frac{Q_2}{\sigma(1+\sigma)}\frac{(1+\sigma)\mathrm{Ra}_{stab}(k)-\mathrm{Ra}}{\mathrm{Ra}_{stab}(k)-\mathrm{Ra}}\frac{k^2}{q^2}$$
$$\times\left[1+\frac{Q_1}{Q_2}\frac{\sigma^2}{(1+\sigma)\mathrm{Ra}_{stab}(k)-\mathrm{Ra}}\right]$$
$$(4.21)$$

and

$$C_{\theta\theta}(k,t=0)=\frac{Q_2}{\sigma(1+\sigma)}\frac{\mathrm{Ra}^2}{\mathrm{Ra}_{stab}(k)-\mathrm{Ra}}$$
$$\times\left[1+\sigma\frac{Q_1}{Q_2}\frac{(1+\sigma)\mathrm{Ra}_{stab}(k)-\mathrm{Ra}}{\mathrm{Ra}^2}\right].$$
$$(4.22)$$

Within the GLE approximation one finds from Eq. (4.11) that

$$C_{ww}^{GLE}(k,t=0)=\frac{Q_2}{3\sigma(1+\sigma)}\left(1+\frac{Q_1}{Q_2}\frac{\sigma^2}{\mathrm{Ra}_c}\right)$$
$$\times\left[\frac{1}{|\epsilon-\xi_0^2(k-k_c)^2|}+\frac{1}{|\epsilon-\xi_0^2(k+k_c)^2|}\right]$$
$$(4.23)$$

and

$$C_{\theta\theta}^{GLE}(k,t=0)=\frac{\mathrm{Ra}_c^2}{q_c^4}\,C_{ww}^{GLE}(k,t=0). \qquad (4.24)$$

Also here for the total spectral weights $C(k,t=0)$ the contributions $\sim Q_1$ from forcing due to stochastic heat currents is small in comparison to the forcing due to stochastic stresses.

$C(k,t=0)$ diverges at the marginal stability boundaries $\mathrm{Ra}_{stab}(k)$ of the HE or $\epsilon_{stab}=\xi_0^2(k-k_c)^2$ of the GLE approximation, respectively (see Fig. 5). At $k=0$ incompressibility does not allow momentum currents in z direction. Therefore C_{ww} (and also $C_{\theta\theta}$ for $Q_1=0$) vanishes $\propto k^2$ for
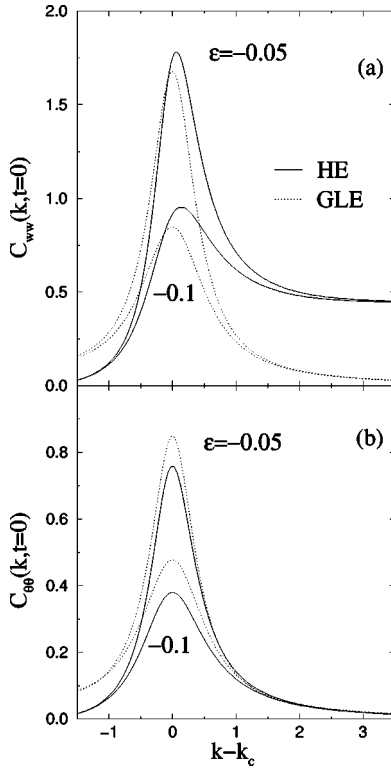
FIG. 5. Wave-number dependence of the reduced total spectral weight in frequency space, $C(k,t=0)$, of velocity fluctuations (a) and of temperature fluctuations (b) according to the hydrodynamic equations (full lines) in comparison with the GLE approximation (dotted lines) for two different driving ϵ as indicated. $C_{ww}(C_{\theta\theta})$ is reduced by $2Q_2$ $(0.02\, Q_2\, \mathrm{Ra}^2)$. Both are independent of the through-flow for free-slip horizontal boundary conditions, c.f. text. The Prandtl number is $\sigma=1$.

small k that cannot be reproduced within the GLE. The dominant contribution $\sim Q_2$ to $C_{\theta\theta}(k,t=0)$ comes from the stochastic momentum currents that distort the vertical temperature stratification. Nevertheless, the forcing by stochastic heat currents $\sim Q_1$ yields a small but finite value of $C_{\theta\theta}$ for large as well as small k.

The most conspicuous difference between the GLE approximation and the hydrodynamic result is the large-k behavior of $C_{ww}(k,t=0)$ and $C_{\theta\theta}(k,t=0)$. The mean square of the stochastic forces that generate fluctuations increases within the theory of fluctuating hydrodynamics quadratically with k. This leads for large k to unphysical behavior in the small-k hydrodynamic theory (cf. the discussion in Sec. III B). Within the GLE, however, the stochastic forces excite all Fourier modes with the same amplitude with which the critical mode is forced. Thus the total GLE-mode intensities of fields drop to zero at large k.

V. SEMI-INFINITE SYSTEMS

In this section we investigate how the fluctuation spectra of the hydrodynamic fields $\Psi(x,\omega)$ [Eq. (2.20b)] are influenced by the fact that the system is taken to be semi-infinite, $0 \leq x < \infty$, and by the specific boundary conditions imposed at $x=0$. In particular, we evaluate how the correlation spec-

tra of the fluctuations taken at a common position x, i.e., the mean-squared fluctuation amplitudes vary with distance x from the inlet.

A. Spatial Laplace transformation

The fluctuating fields $\Psi(x,\omega)$ that enter into the spectra depend (i) on the fluctuating hydrodynamic forces $\xi(x,\omega)$ and (ii) on the boundary conditions at the inlet, $x=0$. To keep track of these two different dependencies we found it convenient to use spatial Laplace transformations according to

$$f(x) \leftrightarrow f(K) = -i \int_0^\infty dx\, e^{-iKx} f(x), \qquad (5.1)$$

with K being a complex wave number. Thus the 6×6 system (2.20) of differential equations

$$[\mathcal{M}(\omega) - \partial_x]\Psi(x,\omega) = \xi(x,\omega) \qquad (5.2\mathrm{a})$$

for the field vector $\Psi(x,\omega)$ [Eq. (2.20b)] reads after Laplace transformation

$$[\mathcal{M}(\omega) - iK]\Psi(K,\omega) = \xi(K,\omega) + i\Psi(x=0,\omega). \qquad (5.2\mathrm{b})$$

The use of spatial Laplace transformations provides an additional computational convenience since it allows to evaluate correlation functions of the fields $\Psi(K,\omega)$ in Laplace space algebraically thus circumventing involved differential and integral operations.

B. Diagonalization

To solve the inhomogeneous boundary value problem (5.2) we diagonalize it with the 6×6 matrix $\mathcal{T}(\omega)$ that diagonalizes $\mathcal{M}(\omega)$ [Eq. (2.20d)] i.e.,

$$(\mathcal{T}^{-1}\mathcal{M}\mathcal{T})_{jk} = iK_j\, \delta_{jk}, \qquad (5.3)$$

where $K_j(\omega)$ $(j=1,\ldots,6)$ are the six spatial eigenvalues discussed in Sec. III A. The matrix $\mathcal{T}$ consisting of the six eigenvectors Ξ_j of $\mathcal{M}$ is a function of the $K_j(\omega,\mathrm{Ra},\mathrm{Pe})$. In the following we sometimes suppress also ω in the argument list. Introducing transformed field vectors φ and force vectors ζ, respectively, by

$$\varphi = \mathcal{T}^{-1}\Psi, \quad \zeta = \mathcal{T}^{-1}\xi, \qquad (5.4)$$

the 6×6 system (5.2) of coupled equations is transformed into six decoupled equations

$$(iK_j - \partial_x)\varphi_j(x) = \zeta_j(x), \qquad (5.5\mathrm{a})$$

$$(iK_j - iK)\varphi_j(K) = \zeta_j(K) + i\varphi_j(x=0), \qquad (5.5\mathrm{b})$$

for the transformed fields φ_j $(j=1,\ldots,6)$. Their respective solution is

$$\varphi_j(x) = e^{iK_j x}\left[\varphi_j(x=0) - \int_0^x dx'\ e^{-iK_j x'}\zeta_j(x')\right],$$
$$(5.6a)$$

$$\varphi_j(K) = \frac{i\ \zeta_j(K) - \varphi_j(x=0)}{K - K_j}.$$
$$(5.6b)$$

From Eq. (5.6) one can obtain the solution of the original fields $\boldsymbol{\Psi}$ by using the inverse transformation of Eq. (5.4)

$$\boldsymbol{\Psi} = \mathcal{T}\boldsymbol{\varphi},\quad \boldsymbol{\xi} = \mathcal{T}\boldsymbol{\zeta}.\qquad(5.7)$$

In this way the solution in Laplace space

$$\boldsymbol{\Psi}(K) = \mathcal{G}(K)[i\boldsymbol{\xi}(K) - \boldsymbol{\Psi}(x=0)]\qquad(5.8a)$$

takes the form of the propagator matrix $\mathcal{G}$ multiplying the inhomogeneity $i\boldsymbol{\xi}(K) - \boldsymbol{\Psi}(x=0)$ where

$$\mathcal{G}(K,\omega) = \mathcal{T}(\omega)\tilde{\mathcal{G}}(K,\omega)\mathcal{T}^{-1}(\omega),\quad \tilde{\mathcal{G}}_{jl}(K,\omega) = \frac{\delta_{jl}}{K - K_j(\omega)}.$$
$$(5.8b)$$

Here $\tilde{\mathcal{G}}$ is the diagonal propagator matrix entering into Eq. (5.6b). In real space the solution (5.8a) reads

$$\boldsymbol{\Psi}(x) = -\mathcal{G}(x)\,\boldsymbol{\Psi}(x=0) + \int_0^x dx'\,\mathcal{G}(x-x')\,\boldsymbol{\xi}(x').$$
$$(5.8c)$$

The propagator matrix

$$\mathcal{G}(x,\omega) = \mathcal{T}(\omega)\,\tilde{\mathcal{G}}(x,\omega)\,\mathcal{T}^{-1}(\omega),\quad \tilde{\mathcal{G}}_{jl}(x,\omega) = -\delta_{jl}\,e^{iK_j(\omega)x}$$
$$(5.9)$$

in real space is the Laplace transform of Eq. (5.8b).

C. Boundary conditions

Not all boundary conditions $\Psi_j(x=0) = \Sigma_{l=1}^6 \mathcal{T}_{jl}\,\varphi_l(x=0)$ are *physically* admissible in the mathematically unrestricted solution (5.6) and (5.7). The *physical* solution $\boldsymbol{\Psi}(x) = \mathcal{T}\boldsymbol{\varphi}(x)$ has to remain finite for all $0 < x < \infty$ as long as the driving is subcritical, $\epsilon < 0$. Thus, in view of the nonsingular form of the transformation matrix $\mathcal{T}(\omega)$ one has to demand that $\varphi_j(x\to\infty)$ remains finite for *all* $j=1,\ldots,6$ when $\epsilon < 0$. This is automatically guaranteed for $p=1,3,5$ [43] for which $\mathrm{Im}\,K_p > 0$. However, for $m=2,4,6$ one would have exponential growth with $\mathrm{Im}\,K_m < 0$ if $\varphi_m(x=0)$ is not chosen appropriately. To avoid a divergence in Eq. (5.6a) for $x\to\infty$ in the subcritical driving regime one has to require that

$$\lim_{x\to\infty}\left[\varphi_m(x=0) - \int_0^x dx'\ e^{-iK_m x'}\zeta_m(x')\right] = 0,$$
$$(5.10a)$$

or equivalently

$$\varphi_m(x=0) = i\ \zeta_m(K_m)\qquad(5.10b)$$

for $m=2,4,6$. Thus, the boundary condition for $\varphi_m(x=0)$ being constrained by a physical nondivergence condition on the fields $\varphi_m(x\to\infty)$ is fixed by the spatial Laplace transform of the fluctuating force ζ_m [Eq. (5.10b)] evaluated for the complex wave number K_m. Inserting the condition (5.10b) into the solution (5.6b) for $m=2,4,6$ one sees that the physically admissible fields

$$\varphi_m(K) = i\ \frac{\zeta_m(K) - \zeta_m(K_m)}{K - K_m}\qquad(5.11)$$

do not contain poles at the three complex wave numbers K_m ($m=2,4,6$) lying in the lower complex half plane. This condition is a direct extension of the result obtained [11] for the case of the GLE. So the residue, $\lim_{K\to K_m}(K-K_m)\,\boldsymbol{\varphi}(K)$, of the poles at K_m ($m=2,4,6$) in the field $\boldsymbol{\varphi}(K)$—and with it also in the field $\boldsymbol{\Psi}(K)$—are zero. When the driving crosses over into the supercritical range $0 < \epsilon < \epsilon^c_{conv}$ then the wave number K_1 (K_3) crosses into the lower complex wave-number plane for ω close to ω_c ($-\omega_c$) leading to exponential growth in positive x direction as discussed in Sec. III. Moreover, only the characteristic "critical" exponents $K_{1,3}$ cause supercritical growth in the driving range $0 < \epsilon < \epsilon^c_{conv}$.

We should like to stress that the nondivergence condition (5.10) fixes only three of the six boundary conditions; the other three boundary conditions are still free to be chosen. Thus with $\varphi_{2,4,6}(x=0)$ being fixed one can choose $\varphi_{1,3,5}(x=0)$ in an arbitrary way so that six conditions on $\Psi_j(x=0)$ ($j=1,\ldots,6$) would result via $\boldsymbol{\Psi} = \mathcal{T}\boldsymbol{\varphi}$ from this choice. However, we can also externally fix three of the Ψ_j fields at the inlet instead, say, $\Psi_4 = u$, $\Psi_5 = w$, and $\Psi_6 = \theta$. The other three $\Psi_{1,2,3}$ would then be determined by the conditions (5.10) together with $\Psi_{4,5,6}$ (cf. Appendix A). This will be done in Sec. V E 1.

D. Decomposition of the fields φ

Before we impose in the next subsection boundary conditions on the original fields $\boldsymbol{\Psi}$ and evaluate their correlation functions we treat first the more simple case of imposing external conditions on three of the transformed fields $\boldsymbol{\varphi}$. As shown in the previous section $\varphi_m(x=0) = i\ \zeta_m(K_m)$ is fixed internally by bulk forcing properties for $m=2,4,6$. The boundary conditions $\varphi_p(x=0)$ ($p=1,3,5$) on the other three fields are still free. Here we consider the inlet boundary conditions $\varphi_p(x=0,\omega)$ ($p=1,3,5$) to be chosen externally and to be statistically independent from the bulk forces. Then the six solutions φ_j [Eq. (5.6)] can be decomposed

$$\boldsymbol{\varphi}(K) = \boldsymbol{\varphi}^{in}(K) + \boldsymbol{\varphi}^b(K)\qquad(5.12a)$$

into an inlet driven part

$$\varphi_j^{in}(K) = \begin{cases} -\dfrac{\varphi_p(x=0)}{K-K_p} & \text{if } j=p=1,3,5 \\[2mm] 0 & \text{if } j=m=2,4,6, \end{cases}\qquad(5.12b)$$

depending only on the externally imposed boundary condition at the inlet and into a bulk driven part

$$
\varphi_j^b(K) = \begin{cases} i\,\dfrac{\zeta_p(K)}{K - K_p} & \text{if } j = p = 1,3,5 \\[2ex] i\,\dfrac{\zeta_m(K) - \zeta_m(K_m)}{K - K_m} & \text{otherwise.} \end{cases}
$$
(5.12c)

In real space one has

$$
\varphi_j^{in}(x) = \begin{cases} e^{iK_p x}\,\varphi_p(x=0) & \text{if } j = p = 1,3,5 \\[1ex] 0 & \text{if } j = m = 2,4,6, \end{cases}
$$
(5.13a)

$$
\varphi_j^b(x) = \begin{cases} -e^{iK_p x} \displaystyle\int_0^x dx'\, e^{-iK_p x'}\,\zeta_p(x') & \text{if } j = p = 1,3,5 \\[2ex] e^{iK_m x} \displaystyle\int_x^\infty dx'\, e^{-iK_m x'}\,\zeta_m(x') & \text{otherwise.} \end{cases}
$$
(5.13b)

Thus the inlet-sustained part is supported only by the inlet boundary condition $\varphi_p(x=0)$ and describes its propagation into the bulk, $x>0$. The bulk part of the fields $\varphi_p^b(x)$ ($p=1,3,5$) is sustained and determined by the fluctuating forces $\zeta_p(x' \leq x)$ to the left of the observation location—the effect of the perturbation at location x' is propagated to the right, i.e., towards the observation point x with the ''propagator'' $e^{iK_p(x-x')}$. On the other hand, fluctuations of the fields $\varphi_m^b(x)$ ($m=2,4,6$) are generated and determined by forces $\zeta_m(x' \geq x)$ operating to the right of the observation location. Here the response is propagated to the left towards the observation point x with the ''propagator'' $e^{-iK_m(x'-x)}$. This again clearly shows the different physical roles (cf. Sec. III) that the characteristic exponents K_p and K_m play: The former, $p=1,3,5$ (latter, $m=2,4,6$) describe downstream (upstream) propagation of perturbations to the right (left).

E. Decomposition of the fields $\mathbf{\Psi}$

We consider now the situation where boundary conditions are imposed externally at the inlet $x=0$ on three of the original hydrodynamic fields $\Psi_j(x,\omega)$ [Eq. (2.20b)]. The other three boundary conditions are fixed by bulk forcing via the nondivergence requirement (5.10).

1. Boundary conditions $\Psi_j(x=0,\omega)$

For the sake of definiteness we impose *externally* determined boundary conditions on the three fields $\Psi_4=u, \Psi_5=w, \Psi_6=\theta$. Then the boundary conditions on the remaining three fields $\Psi_{1,2,3}(x,\omega)$ can be separated into two parts,

$$
\Psi_{1,2,3}(x=0,\omega) = \Psi_{1,2,3}^{in}(x=0,\omega) + \Psi_{1,2,3}^b(x=0,\omega),
$$
(5.14a)

with

$$
\begin{pmatrix} \Psi_1^{in} \\ \Psi_2^{in} \\ \Psi_3^{in} \end{pmatrix} = A \begin{pmatrix} \Psi_4 \\ \Psi_5 \\ \Psi_6 \end{pmatrix}, \quad \begin{pmatrix} \Psi_1^b \\ \Psi_2^b \\ \Psi_3^b \end{pmatrix} = B \begin{pmatrix} \zeta_2(K_2) \\ \zeta_4(K_4) \\ \zeta_6(K_6) \end{pmatrix}
$$
(5.14b)

at $x=0$ according to Eq. (A4) in Appendix A. The 3×3 matrices $A(\omega)$ and $B(\omega)$ [Eq. (A5)] contain matrix elements of $\mathcal{T}(\omega)$ and $\mathcal{T}^{-1}(\omega)$. Note that the contribution $\Psi_{1,2,3}^{in}(x=0,\omega)$ contains only the externally controlled boundary conditions $\Psi_{4,5,6}(x=0,\omega)$ at the inlet. The bulk part $\Psi_{1,2,3}^b(x=0,\omega)$ ensures the nondivergence condition. It is in this way that the bulk forcing $\zeta_m(K_m) = \Sigma_{j=1}^6 (\mathcal{T}^{-1})_{mj}\xi_j(K_m)$ enters into the boundary condition $\Psi_{1,2,3}(x=0,\omega)$.

Since the field components $\Psi_{4,5,6}(x=0,\omega)$ are chosen to be genuinely externally determined at the inlet we have

$$
\Psi_{4,5,6}(x=0,\omega) = \Psi_{4,5,6}^{in}(x=0,\omega), \quad \Psi_{4,5,6}^b(x=0,\omega) = 0
$$
(5.15)

in our notation.

2. Field decomposition

With the decomposition (5.14) and (5.15) of the boundary conditions one can immediately decompose also the fields $\mathbf{\Psi}(K)$ [Eq. (5.8)] into

$$
\mathbf{\Psi}(K,\omega) = \mathbf{\Psi}^{in}(K,\omega) + \mathbf{\Psi}^b(K,\omega),
$$
(5.16a)

with

$$
\mathbf{\Psi}^{in}(K,\omega) = -\mathcal{G}(K,\omega)\mathbf{\Psi}^{in}(x=0,\omega),
$$
(5.16b)

$$
\mathbf{\Psi}^b(K,\omega) = \mathcal{G}(K,\omega)[i\boldsymbol{\xi}(K,\omega) - \mathbf{\Psi}^b(x=0,\omega)].
$$
(5.16c)

Here $\mathbf{\Psi}^{in}(K,\omega)$ is supported only by the externally imposed inlet boundary conditions that enter directly into $\Psi_{4,5,6}^{in}(x=0,\omega)$ [Eq. (5.15)] and indirectly into $\Psi_{1,2,3}^{in}(x=0,\omega)$ [Eq. (5.14b)]. The bulk part $\mathbf{\Psi}^b$ is determined solely by the fluctuating forces $\boldsymbol{\xi}$ that enter directly into Eq. (5.16c) and in addition indirectly into $\Psi_{1,2,3}^b(x=0,\omega)$ [Eq. (5.14b)] via the nondivergence constraint. In real space one has

$$
\mathbf{\Psi}(x,\omega) = \mathbf{\Psi}^{in}(x,\omega) + \mathbf{\Psi}^b(x,\omega),
$$
(5.17a)

with

$$
\mathbf{\Psi}^{in}(x,\omega) = -\mathcal{G}(x,\omega)\mathbf{\Psi}^{in}(x=0,\omega),
$$
(5.17b)

$$
\mathbf{\Psi}^b(x,\omega) = \int_0^x dx'\, \mathcal{G}(x-x',\omega)\,\boldsymbol{\xi}(x',\omega)
$$
$$
- \mathcal{G}(x,\omega)\mathbf{\Psi}^b(x=0,\omega).
$$
(5.17c)

Note that Eq. (5.16) or (5.17) together with Eqs. (5.14) and (5.15) is the complete physical solution for the fields $\mathbf{\Psi}(\omega)$ that is constructed such as to explicitly obey the externally imposed and the implicitly physically required boundary conditions. The propagator matrix $\mathcal{G}(K,\omega)$ [Eq. (5.8b)] entering into $\mathbf{\Psi}^{in}(K,\omega)$ [Eq. (5.16b)] contains poles

at all six locations in the complex plane given by the characteristic spatial eigenvalues K_j. However, $\Psi(x=0)$ was designed to ensure that the residues of the poles of $\Psi(K)$ in the lower complex half plane at K_m ($m=2,4,6$) are zero for arbitrarily chosen $\Psi_{4,5,6}(x=0)$ and arbitrary realizations of forces $\xi(K)$. Thus each of the contributions, $\Psi^{in}(K)$ as well as $\Psi^b(K)$, do not contain poles at $K_{2,4,6}$ separately. Therefore only spatial variations $\sim e^{iK_p x}$ ($p=1,3,5$) occur in $\Psi^{in}(x,\omega)$ (5.17b). Moreover, the terms $\sim e^{iK_m x}$ ($m=2,4,6$) in $\Psi^b(x,\omega)$ [Eq. (5.17c)] play only the role of ''propagators'' in the upstream direction as seen already in the simpler case of Sec. V D.

F. Decomposition of correlation functions

Here we evaluate the correlation function matrix

$$C_{ij}(x,\omega;x',\omega')=\langle\Psi_i(x,\omega)[\Psi_j(x',\omega')]^*\rangle \quad (5.18)$$

for the case that the boundary conditions $\Psi_{4,5,6}(x=0,\omega)$ for the fields u,w,θ that are imposed externally at the inlet are statistically independent from the bulk forces $\xi(x,\omega)$. After all, these forces were assumed to be δ correlated in space. Then the field Ψ^{in} is uncorrelated with the bulk part Ψ^b. Consequently, the correlation matrix (5.18) splits into an inlet part and into a bulk part

$$C_{ij}=C_{ij}^{in}+C_{ij}^b. \quad (5.19)$$

Here $C_{ij}^{in}=\langle\Psi_i^{in}[\Psi_j^{in}]^*\rangle$ contains correlations of Ψ^{in} [Eq. (5.17b)] while $C_{ij}^b=\langle\Psi_i^b[\Psi_j^b]^*\rangle$ contains correlations of the field Ψ^b [Eq. (5.17c)] only.

$C_{ij}(x,\omega;x,\omega')$ contains the factor $2\pi\delta(\omega-\omega')$. It follows from the fact that the forcing process $\xi(x,t)$, as well as the boundary conditions $\Psi_{4,5,6}(x=0,t)$ are taken as statistically stationary and that in the considered long-time limit initial-value dependencies have relaxed away. Note, however, that the process $\Psi(x,t)$ is spatially not translational invariant due to the boundary at $x=0$. Thus Eq. (5.18) depends on x and x' separately.

1. Inlet part

The inlet part of the correlation matrix

$$C^{in}(x,\omega;x',\omega')=\mathcal{G}(x,\omega)\mathcal{D}(\omega,\omega')\mathcal{G}^\dagger(x',\omega') \quad (5.20)$$

is given by the propagator matrix $\mathcal{G}$ (5.9) and its Hermitian adjoint $\mathcal{G}^\dagger$ multiplying the correlation function matrix

$$\mathcal{D}_{jj'}(\omega,\omega')=\langle\Psi_j^{in}(x=0,\omega)[\Psi_{j'}^{in}(x=0,\omega')]^*\rangle \quad (5.21)$$

of the field $\Psi^{in}(x=0,\omega)$. The latter is determined according to [Eqs. (5.14b) and (5.15)] by the externally imposed field components $\Psi_{4,5,6}(x=0,\omega)$. The case of nonstochastic inlet conditions is included as a special case in Eq. (5.21) as well; in particular, also the trivial case of $\Psi^{in}(x=0,\omega)=0$ where $\mathcal{D}=C^{in}=0$.

Consider now the spectrum

$$C_{ij}^{in}(x,\omega)=\frac{C_{ij}^{in}(x,\omega;x,\omega')}{2\pi\,\delta(\omega-\omega')} \quad (5.22)$$

of the correlation matrix (5.20) taken at the common position x. Into its spatial evolution there enter only the three exponentials $e^{iK_p x}$ ($p=1,3,5$) as explained at the end of Sec. V E. Thus if the driving is in the convectively unstable regime where $\mathrm{Im}\,K_{1,3}$ become negative the spectrum (5.22) is dominated for positive ω at large x by the growth behavior

$$C_{ij}^{in}(x,\omega)\simeq E_{ij}(\omega)e^{-2\,\mathrm{Im}\,K_1(\omega)x}, \quad (5.23a)$$

resulting from $e^{iK_1 x}$. For $\omega<0$ the growth is dominated by $\mathrm{Im}\,K_3(\omega)=\mathrm{Im}\,K_1(-\omega)$. The matrix

$$E(\omega)=\mathcal{S}(\omega)\frac{\mathcal{D}(\omega,\omega')}{2\pi\,\delta(\omega-\omega')}\mathcal{S}^\dagger(\omega) \quad (5.23b)$$

is given by the inlet correlation matrix (5.21) and

$$\mathcal{S}_{ij}(\omega)=\mathcal{T}_{i1}(\omega)\,\mathcal{T}_{1j}^{-1}(\omega). \quad (5.23c)$$

In the subcritical driving range $\epsilon<0$, where $\mathrm{Im}\,K_p>0$ for all $p=1,3,5$ all correlation spectra $C^{in}(x,\omega)$ [Eq. (5.22)] decay to zero for $x\to\infty$. Their decay is dominated by the imaginary part of the characteristic exponent K_p that is closest to the real axis in complex wave-number space. For positive ω (and Pe) this is K_1 when ϵ is only slightly subcritical.

2. Bulk part

The evaluation of the bulk part

$$C_{jj'}^b(x,\omega;x',\omega')=\langle\Psi_j^b(x,\omega)[\Psi_{j'}^b(x',\omega')]^*\rangle \quad (5.24)$$

of the correlation matrix is more complicated since the fluctuating forces ξ enter into the first term of Ψ^b [Eqs. (5.16c) and (5.17c)] explicitly and into the second term implicitly via the condition $\Psi_{1,2,3}^b(x=0)$. The latter reads, e.g., for

$$\Psi_1^b(x=0)=B_{1m}\zeta_m(K_m)=B_{1m}\mathcal{T}_{mj}^{-1}\xi_j(K_m) \quad (5.25)$$

according to Eq. (5.14b) with $B(\omega)$ given in Appendix A. In Eq. (5.25) sums over $m=2,4,6$ and $j=1,2,\ldots,6$ are implied. Thus the stochastic forces enter into $\Psi_{1,2,3}^b(x=0)$ via their Laplace transformation.

Instead of directly evaluating Eq. (5.24) in real space we preferred the algebraic method of determining the correlation matrix in Laplace space,

$$C_{jj'}^b(K,\omega;K',\omega')=\langle\Psi_j^b(K,\omega)\hat{\Psi}_{j'}^b(K',\omega')\rangle, \quad (5.26)$$

and then perform a double-Laplace transform back to real space. The rational functions of K,K' appearing in Eq. (5.26) can easily be transformed back, say, with MATHEMATICA. In Eq. (5.26) and in the following we denote for better identification of the two functions entering into Eq. (5.24) the Laplace transform of a function $[f(x)]^*$ by an additional caret, i.e.,

$$[f(x)]^* \leftrightarrow \hat{f}(K) = -[f(-K^*)]^*, \qquad (5.27)$$

where $f(x) \leftrightarrow f(K)$.

In order to give an impression of the algebraical problems involved in Eq. (5.26) we introduce the auxiliary effective forcing field

$$\boldsymbol{\xi}^{eff}(K,\omega) = \boldsymbol{\xi}(K,\omega) + i\boldsymbol{\Psi}^b(x=0,\omega) \qquad (5.28)$$

in order to keep the expressions handy. The choice of the superscript *eff* for effective is motivated by the fact that $\Psi^b_{1,2,3}(x=0,\omega)$ is given by the stochastic bulk forces $\boldsymbol{\xi}(K_m)$ ($m=2,4,6$) as indicated in Eq. (5.25). Then one finds with $\boldsymbol{\Psi}^b(K,\omega) = i\mathcal{G}(K,\omega)\,\boldsymbol{\xi}^{eff}(K,\omega)$ that

$$\mathcal{C}^b_{jj'}(K,\omega;K',\omega')$$
$$= \mathcal{G}_{jl}(K,\omega) \langle \xi^{eff}_l(K,\omega)\,\hat{\xi}^{eff}_{l'}(K',\omega') \rangle \hat{\mathcal{G}}_{j'l'}(K',\omega').$$
$$(5.29)$$

With $\boldsymbol{\xi}^{eff}$ being linearly related via Eqs. (5.28) and (5.25) to $\boldsymbol{\xi}$ one can express the correlation function of $\boldsymbol{\xi}^{eff}$ entering into Eq. (5.29) in terms of the forcing correlation matrix (Appendix B)

$$\mathcal{F}_{jj'}(Q,\omega;Q',\omega') = \langle \xi_j(Q,\omega)\,\hat{\xi}_{j'}(Q',\omega') \rangle$$
$$= 2\pi\,\delta(\omega-\omega')\frac{\mathcal{N}_{jj'}(Q,Q')}{Q+Q'}.$$
$$(5.30)$$

Here Q denotes either K or $K_{2,4,6}$ and Q' stands for either K' or $K_{2,4,6}$. The matrix $\mathcal{N}$ [Eq. (B3)] in the numerator of Eq. (5.30) contains Q and Q' up to bilinear order QQ'. The propagator matrix $\mathcal{G}$ entering into Eq. (5.29) contains sums of simple pole terms $\sim 1/(K-K_j)$. Thus one can apply partial fraction decompositions and the method of residues in the double-Laplace transform of Eq. (5.29) back to real space.

G. Correlation spectra

Let us discuss the spatial evolution of the correlation spectra of the temperature fluctuations $\theta(x,\omega) = \Psi_6(x,\omega)$ as a representative example. Those of w are quite similar to those of θ; and w and u are related to each other via incompressibility (2.18a).

The inlet part [Eqs. (5.20)–(5.23)] is essentially dominated for positive ω by the contribution from the growth/decay behavior $e^{iK_1 x}$ coming from the "critical" characteristic exponent K_1 as discussed in Sec. V F 1. So we concentrate here on the bulk part

$$C^b_{ij}(x,\omega) = \frac{\langle \Psi^b_i(x,\omega)[\Psi^b_j(x,\omega')]^* \rangle}{2\pi\,\delta(\omega-\omega')} \qquad (5.31)$$

of the spectrum of fluctuations taken at a common position $x=x'$.

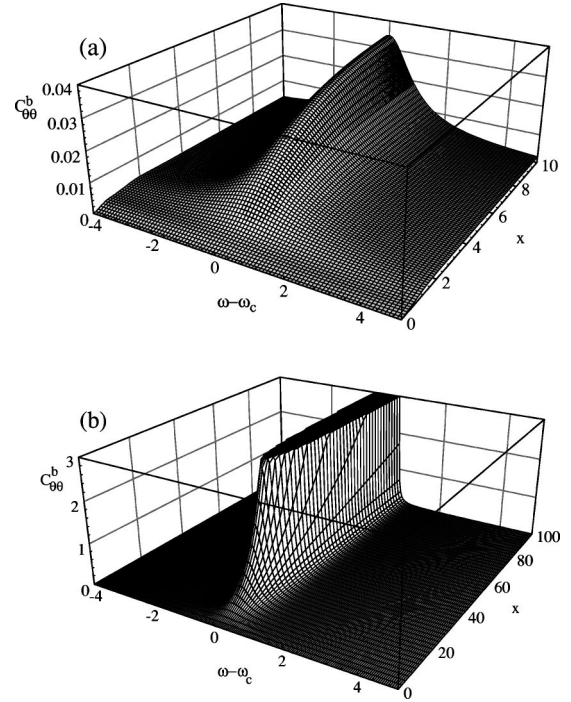Figure 6(a) shows the bulk-generated part $C^b_{\theta\theta}(x,\omega)$ of

FIG. 6. Bulk part $C^b_{\theta\theta}(x,\omega)$ of the correlation spectrum of temperature fluctuations in a semi-infinite system with through-flow Péclet number Pe=2 subject to the boundary condition $\theta^b(x=0,\omega)=0$. For the subcritical driving $\epsilon=-0.05$ (a) $C^b_{\theta\theta}$ grows in downstream direction to a finite bulk level depending on frequency ω. For the supercritical driving $\epsilon=0.016$ (b) the correlation spectrum diverges $\propto e^{-2\,\mathrm{Im}\,K_1(\omega)x}$ within the frequency band ($\omega_c-0.47$, $\omega_c+0.52$). $C^b_{\theta\theta}$ is reduced by $\mathrm{Ra}^2 Q_2/2\pi$. The Prandtl number is $\sigma=1$.

the spectrum as a three dimensional plot over the $x-\omega$ plane of variables for a slightly subcritical driving ($\epsilon=-0.05$) with through-flow, Pe=2. The critical frequency is $\omega_c = k_c\,\mathrm{Pe}$. With the decomposition of the fields $\boldsymbol{\Psi}$ into externally and internally generated parts one has $\Psi^b_6(x=0) = \theta^b(x=0) = 0$ Eq. (5.15) so that $C^b_{\theta\theta}(x=0,\omega) = 0$. On the other hand, for $x \to \infty$ the bulk-generated temperature fluctuation spectrum approaches in the subcritical driving situation a finite limit spectrum $C^b_{\theta\theta}(x=\infty,\omega)$. The latter is the same as the wave-number integral, $\int_{-\infty}^{\infty} (dk/2\pi) C_{\theta\theta}(k,\omega)$, Eq. (4.18), over the fluctuation spectrum in doubly infinite systems. The approach to this limit, $\propto (1-e^{-2\mathrm{Im}\,K_1 x})$, is governed by the spatial eigenvalue K_1 that is closest to the real axis. On the other hand, the variation near the inlet is caused by the contribution from the other exponentials.

Figure 6(b) shows $C^b_{\theta\theta}(x,\omega)$ in the convectively unstable regime. The driving is $\epsilon=0.016$. The other parameters are the same as in Fig. 6(a). Here the correlation spectrum $C^b_{\theta\theta}(x,\omega)$ diverges $\sim e^{-2\,\mathrm{Im}\,K_1 x}$ for large x in the critical band $\omega_c-0.47 < \omega < \omega_c+0.52$ of negative $\mathrm{Im}\,K_1(\omega)$. Mean-squared fluctuations with the critical frequency ω_c have the highest downstream growth at the inlet and are dominated by the eigenvalue K_1. Outside the critical-frequency band all perturbations are damped.

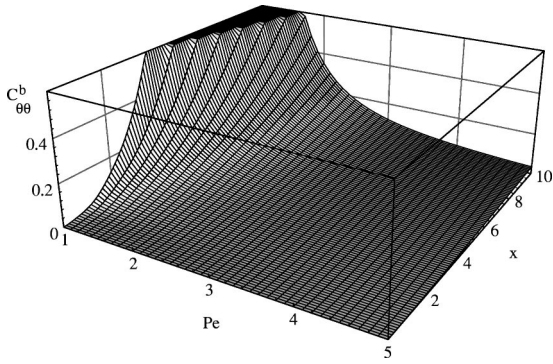The influence of through-flow on the growth length of

FIG. 7. Bulk-generated mean-squared temperature fluctuations $C_{\theta\theta}^b(x,\omega_c,\text{Pe})$ with critical frequency ω_c as a function of downstream distance x from the inlet and through-flow Péclet number Pe for $\epsilon=0.016$ in the convectively unstable regime. The large-x behavior is dominated by $e^{-2\,\text{Im}\,K_1(\omega_c,\text{Pe})x}$. $C_{\theta\theta}^b$ is reduced by $\text{Ra}^2 Q_2/2\pi$. The Prandtl number is $\sigma=1$.

bulk fluctuations with ω_c is presented in Fig. 7. At the supercritical heating $\epsilon=0.016$ the correlation spectra $C_{\theta\theta}^b(x,\omega_c)$ are shown for increasing group velocities Pe of convectively unstable states. The through-flow expands the influence of the inlet conditions [in our case $\theta^{in}(x=0,\omega)=0$] into the bulk. Thus higher the Pe the longer is the growth length of mean-temperature fluctuations since the downstream variation $\sim e^{-2\,\text{Im}\,K_p x}$ ($p=1,3,5$) flattens and the upstream modes $\sim e^{iK_m x}$ ($m=2,4,6$) decay faster in upstream direction.

VI. CONCLUSIONS

We have studied fluctuations of the hydrodynamic fields in laterally infinite and semi-infinite Rayleigh-Bénard systems with lateral through-flow in the vicinity of the threshold for onset of convection. The linearized field equations including additive thermal forcing have been projected into the subspace with the critical variation in z and y directions for free-slip horizontal boundaries.

In addition to the standard temporal growth analysis of modes $\sim e^{ikx}$, with real k we have studied the spatial response $\sim e^{iK(\omega)x}$ of an oscillatory mode $e^{-i\omega t}$ with real ω. There are six different characteristic spatial exponents $K_j(\omega)$. Their imaginary parts determine the spatial growth or decay of the modes. In the subcritical driving regime, $\epsilon<0$, three of them—namely, $K_{1,3,5}$ ($K_{2,4,6}$) in our notation—lie in the upper (lower) complex wave-number plane. The contributions $\sim e^{iK_{1,3,5}x}$ ($e^{iK_{2,4,6}x}$) determine the evolution of the fields to the right (left), i.e., in downstream (upstream) direction for through-flow in positive x direction. With increasing through-flow the downstream (upstream) growth lengths $1/\text{Im}\,K_{1,3,5}$ ($-1/\text{Im}\,K_{2,4,6}$) increase (decrease). When the Rayleigh number becomes supercritical the ''critical'' eigenvalues K_1 and K_3 cross the real axis at $k=\pm k_c$ with $\omega=\pm\omega_c$, respectively, for $\epsilon=0$. Thereafter in the supercritical regime, $0<\epsilon<\epsilon_{conv}^c$ below the boundary ϵ_{conv}^c between the convectively and absolutely unstable driving range all perturbations with frequencies around $\pm\omega_c$ for which $\text{Im}\,K_{1,3}(\omega)<0$ are amplified in downstream direction. The

other eigenvalues do not show such a distinctive behavior close to $\epsilon=0$. The eigenvalues $K_{5,6}$ with relatively large imaginary parts implying large spatial variations are of purely hydrodynamic origin. They do not appear in the GLE approximation. The agreement of both descriptions improves when reducing $|\epsilon|$.

In Sec. IV we have discussed the fluctuation dynamics in unrestricted geometry. By comparing the residue of the correlation functions at $\epsilon\to 0^-$ with the corresponding GLE expressions the stochastic forcing strength γ of the latter could be identified in terms of the strength of stress and heat current fluctuations. For small $|\epsilon|$ the correlation spectra $C_{ww}(k,\omega)$ and $C_{\theta\theta}(k,\omega)$ of velocity and temperature fluctuations, respectively, compare rather well with the GLE approximation with a better agreement in the former case. The total spectral weight $C_{ww}(x=0,\omega)$ in wave-number space deviates with increasing through-flow more and more from the GLE approximation due to substantial contribution from the high-momentum region. In frequency space the corresponding total spectral weights, $C_{ww}(k,t=0)$, for the GLE and HE differ at large k as a result of an overestimated hydrodynamic weight $\propto k^2$.

In Sec. V we have investigated how a restricted geometry and inlet conditions at $x=0$ influence the statistical dynamics of hydrodynamic fluctuations in downstream direction. We have considered a statistically stationary situation with time translational invariant correlations of the fluctuations that are evaluated in ω space. But because of the restricted geometry the system is not translational invariant. Therefore we have used spatial Laplace transformations as a convenient tool to separate the effects of inlet forcing at the boundary, $x=0$, and of bulk thermal forcing. Moreover, this method allows also for an algebraical evaluation of correlation functions having simple pole structures in Laplace space that can straightforwardly be transformed back into real space. The six characteristic spatial exponents mark the pole positions.

The hydrodynamic field equations require six boundary conditions. Three can be imposed freely at the inlet and the other three are chosen such that the fluctuations do not diverge at $x\to\infty$ in the subcritical driving range. These conditions imply that in Laplace space the residue of the poles at $K_{2,4,6}$ in the lower complex half plane vanish. That, in turn, fixes the remaining conditions at $x=0$ in terms of bulk thermal forcing properties. In this way one can separate the contribution to the fluctuating fields and their correlations that are caused by externally imposed boundary conditions at $x=0$ on the one hand and bulk thermal forcing on the other. This decomposition is exemplified for the experimentally relevant situation that the temperature and velocity fields are specified at the inlet.

For subcritical driving $\epsilon<0$, the spectra of the fluctuating fields approach for $x\to\infty$ the corresponding ones in an infinite system $\propto[1-e^{-2\,\text{Im}\,K_1(\omega)x}]$ when ω is close to ω_c. For ω close to $-\omega_c$ it is the other ''critical'' exponent K_3 that dominates the growth. In the supercritical, convectively unstable driving range the fluctuation amplitudes diverge $\propto e^{-2\,\text{Im}\,K_1(\omega)x}$ at large x when ω lies in the band of modes close to ω_c for which $\text{Im}\,K_1(\omega)<0$. Increasing the through-flow causes the growth length of fluctuations to increase.

Experimental investigations [44] of Rayleigh-Bénard convection in the presence of a lateral flow have been done predominantly in the absolutely unstable parameter regime where the convection structures are well developed and largely insensitive to perturbations. While the necessity to distinguish also in this open-flow system between convective and absolute instability [45] is becoming common knowledge, there is a lack of convection experiments that are specifically designed to measure the downstream growth and evolution not only of amplitudes but also of fluctuation spectra of flow intensity and/or temperature. Such experiments, performed in long and narrow convection channels, are best suited to determine the influence of inlet and bulk thermal noise. These data should allow at least a qualitative comparison with our free-slip theoretical results for the spatial evolution of the frequency spectra of the fluctuations.

APPENDIX A: BOUNDARY CONDITIONS AT $x=0$

In Sec. V C we have seen that one has to impose the boundary conditions (5.10) on the fields with $m=2,4,6$ in order to avoid unphysical divergences at $x\rightarrow\infty$ for subcritical driving. With the three even components $m=2,4,6$ of the transformed fields $\boldsymbol{\varphi}=\mathcal{T}^{-1}\boldsymbol{\Psi}$ [Eq. (5.7)] being determined internally at $x=0$ according to Eq. (5.10) by the Laplace transformation of the bulk transformed-field forces $\boldsymbol{\zeta}=\mathcal{T}^{-1}\boldsymbol{\xi}$ the odd components φ_p with $p=1,3,5$ still require a boundary condition at $x=0$.

In this appendix we externally impose as one possible choice boundary values on the fields $\Psi_4=u$, $\Psi_5=w$, and $\Psi_6=\theta$. Then with $\varphi_{2,4,6}(x=0)$ being fixed internally and with $\Psi_{4,5,6}(x=0)$ being fixed externally we explicitly evaluate the remaining other components $\varphi_{1,3,5}(x=0)$ and $\Psi_{1,2,3}(x=0)$ of the transformed and of the untransformed field set, respectively. To that end we decompose the transformation relations $\boldsymbol{\Psi}=\mathcal{T}\boldsymbol{\varphi}$ and $\boldsymbol{\varphi}=\mathcal{T}^{-1}\boldsymbol{\Psi}$ as follows:

$$\begin{pmatrix}\varphi_1\\\varphi_3\\\varphi_5\end{pmatrix}=a\begin{pmatrix}\Psi_4\\\Psi_5\\\Psi_6\end{pmatrix}+b\begin{pmatrix}\Psi_1\\\Psi_2\\\Psi_3\end{pmatrix},\qquad(A1a)$$

$$\begin{pmatrix}\Psi_1\\\Psi_2\\\Psi_3\end{pmatrix}=c\begin{pmatrix}\varphi_2\\\varphi_4\\\varphi_6\end{pmatrix}+d\begin{pmatrix}\varphi_1\\\varphi_3\\\varphi_5\end{pmatrix},\qquad(A1b)$$

$$a=\begin{pmatrix}\mathcal{T}^{-1}_{14}&\mathcal{T}^{-1}_{15}&\mathcal{T}^{-1}_{16}\\\mathcal{T}^{-1}_{34}&\mathcal{T}^{-1}_{35}&\mathcal{T}^{-1}_{36}\\\mathcal{T}^{-1}_{54}&\mathcal{T}^{-1}_{55}&\mathcal{T}^{-1}_{56}\end{pmatrix},\quad b=\begin{pmatrix}\mathcal{T}^{-1}_{11}&\mathcal{T}^{-1}_{12}&\mathcal{T}^{-1}_{13}\\\mathcal{T}^{-1}_{31}&\mathcal{T}^{-1}_{32}&\mathcal{T}^{-1}_{33}\\\mathcal{T}^{-1}_{51}&\mathcal{T}^{-1}_{52}&\mathcal{T}^{-1}_{53}\end{pmatrix},$$

$$(A2a)$$

$$c=\begin{pmatrix}\mathcal{T}_{12}&\mathcal{T}_{14}&\mathcal{T}_{16}\\\mathcal{T}_{22}&\mathcal{T}_{24}&\mathcal{T}_{26}\\\mathcal{T}_{32}&\mathcal{T}_{34}&\mathcal{T}_{36}\end{pmatrix},\quad d=\begin{pmatrix}\mathcal{T}_{11}&\mathcal{T}_{13}&\mathcal{T}_{15}\\\mathcal{T}_{21}&\mathcal{T}_{23}&\mathcal{T}_{25}\\\mathcal{T}_{31}&\mathcal{T}_{33}&\mathcal{T}_{35}\end{pmatrix}.$$

$$(A2b)$$

Combining Eq. (A1b) with Eq. (A1a) one immediately finds the sought-after relations between the fields at $x=0$,

$$\begin{pmatrix}\varphi_1\\\varphi_3\\\varphi_5\end{pmatrix}=(1-bd)^{-1}\,a\begin{pmatrix}\Psi_4\\\Psi_5\\\Psi_6\end{pmatrix}+(1-bd)^{-1}\,bc\begin{pmatrix}\varphi_2\\\varphi_4\\\varphi_6\end{pmatrix},$$

$$(A3)$$

$$\begin{pmatrix}\Psi_1\\\Psi_2\\\Psi_3\end{pmatrix}=(1-db)^{-1}\,da\begin{pmatrix}\Psi_4\\\Psi_5\\\Psi_6\end{pmatrix}+(1-db)^{-1}\,c\begin{pmatrix}\varphi_2\\\varphi_4\\\varphi_6\end{pmatrix}.$$

$$(A4)$$

Comparing this form with Eq. (5.14) we identify

$$A=(1-db)^{-1}da,\quad B=(1-db)^{-1}c.\qquad(A5)$$

Equations (A3) and (A4) show explicitly how the boundary conditions on $\varphi_{1,3,5}$ and on $\Psi_{1,2,3}$ are related to the externally imposed conditions $\Psi_{4,5,6}$ and the internally required conditions $\varphi_{2,4,6}$ involving bulk forces. Note that Eqs. (A3) and (A4) require the matrix $(1-db)$ to be invertible.

We should like to stress here that in general one can fix only three arbitrarily chosen field components out of the six components of the field vector $\boldsymbol{\Psi}$ at the inlet, $x=0$. The remaining three boundary conditions for the system (5.2) of six differential equations of first order are furnished by the conditions (5.10) on $\varphi_{2,4,6}(x=0)$ that ensure the correct physical behavior of the solution at $x\rightarrow\infty$. Thus if one chooses to impose external conditions on three Ψ fields other than $\Psi_{4,5,6}$ one gets in a way that is completely analogous to Eqs. (A1) and (A2) matrix relations that express $\varphi_{1,3,5}$ in terms of $\varphi_{2,4,6}$ and the three chosen Ψ fields and the remaining three Ψ fields in terms of the chosen ones and $\varphi_{2,4,6}$.

APPENDIX B: LAPLACE TRANSFORMED FORCE CORRELATIONS

Here we compile formulas for the double-spatial Laplace transformation of the force correlation functions

$$\langle\xi_j(x,\omega)[\xi_{j'}(x',\omega')]^*\rangle\overset{\leftrightarrow}{\underset{\leftrightarrow}{}}\langle\xi_j(K,\omega)\hat{\xi}_{j'}(K',\omega')\rangle$$

$$=\mathcal{F}_{jj'}(K,\omega;K',\omega').\qquad(B1)$$

Here the caret indicates the Laplace transformation of a conjugate-complex function in real space as introduced in Eq. (5.27). Since $[\boldsymbol{\xi}(x,\omega)]^*=\boldsymbol{\xi}(x,-\omega)$ as a consequence of the reality of $\boldsymbol{\xi}(x,t)$ one has

$$\hat{\xi}_{j'}(K',\omega')=\xi_{j'}(K',-\omega').\qquad(B2)$$

From Eqs. (2.19) and (2.20b) one finds

$$\mathcal{F}_{jj'}(K,\omega;K',\omega')=2\pi\;\delta(\omega-\omega')\,\frac{\mathcal{N}_{jj'}(K,K')}{K+K'} \tag{B3a}$$

with

$$\mathcal{N}_{11}=2i\,\frac{Q_2}{\sigma^2}\left[\left(\frac{\zeta}{\nu\rho}+\frac{4}{3}\right)\pi^2-KK'\right], \tag{B3b}$$

$$\mathcal{N}_{13}=2\,\frac{Q_2}{\sigma}\,\pi\left[K-\left(\frac{\zeta}{\nu\rho}-\frac{2}{3}\right)K'\right], \tag{B3c}$$

$$\mathcal{N}_{22}=2i\,Q_1(\pi^2-KK'), \tag{B3d}$$

$$\mathcal{N}_{31}=2\,\frac{Q_2}{\sigma}\,\pi\left[K'-\left(\frac{\zeta}{\nu\rho}-\frac{2}{3}\right)K\right], \tag{B3e}$$

$$\mathcal{N}_{33}=2i\,Q_2\left[\pi^2-\left(\frac{\zeta}{\nu\rho}+\frac{4}{3}\right)KK'\right], \tag{B3f}$$

and $\mathcal{N}_{jj'}=0$ for all other j,j'. At the inlet, $x=0$, we discard the fluctuating stresses σ_{11} and σ_{33} and the lateral component of the fluctuating heat current. With u,w,θ being fixed at $x=0$ they do not enter into the correlation functions (5.18).

---

[1] M. C. Cross and P. C. Hohenberg, Rev. Mod. Phys. **65**, 851 (1993).

[2] R. J. Deissler, J. Stat. Phys. **40**, 371 (1985); **54**, 1459 (1989); Physica D **25**, 233 (1987).

[3] R. J. Deissler and H. R. Brand, Phys. Lett. A **130**, 293 (1988).

[4] K. L. Babcock, G. Ahlers, and D. S. Cannell, Phys. Rev. Lett. **67**, 3388 (1991); Phys. Rev. E **50**, 3670 (1994); K. L. Babcock, D. S. Cannell, and G. Ahlers, Physica D **61**, 40 (1992).

[5] A. Tsameret and V. Steinberg, Europhys. Lett. **14**, 331 (1991); Phys. Rev. Lett. **67**, 3392 (1991); Phys. Rev. E **49**, 1291 (1994); A. Tsameret, G. Goldner, and V. Steinberg, *ibid.* **49**, 1309 (1994).

[6] H. W. Müller, M. Lücke, and M. Kamps, Phys. Rev. A **45**, 3714 (1992).

[7] W. Schöpf and I. Rehberg, Europhys. Lett. **17**, 321 (1992); J. Fluid Mech. **271**, 235 (1994).

[8] M. Lücke and A. Recktenwald, Europhys. Lett. **22**, 559 (1993).

[9] J. B. Swift, K. L. Babcock, and P. C. Hohenberg, Physica A **204**, 625 (1994).

[10] R. J. Deissler, Phys. Rev. E **49**, R31 (1994).

[11] M. Lücke and A. Szprynger, Phys. Rev. E **55**, 5509 (1997).

[12] S. P. Trainoff, Ph.D. thesis, UCSB, 1997.

[13] A. Bers, in *Basic Plasma Physics I*, edited by A. A. Galeev and R. N. Sudan (North-Holland, New York, 1983).

[14] R. J. Briggs, *Electron-Stream Interaction with Plasmas* (MIT Press, Cambridge, MA, 1964).

[15] P. Huerre, in *Instabilities and Nonequilibrium Structures*, edited by E. Tirapegui and D. Villaroel (Reidel, Dordrecht, 1987), p. 141.

[16] G. Quentin and I. Rehberg, Phys. Rev. Lett. **74**, 1578 (1995).

[17] M. Wu, G. Ahlers, and D. S. Cannell, Phys. Rev. Lett. **75**, 1743 (1995).

[18] L. D. Landau and E. M. Lifshitz, *Fluid Mechanics* (Pergamon, London, 1959).

[19] V. M. Zaitsev and M. I. Shliomis, Zh. Éksp. Teor. Fiz. **59**, 1583 (1970) [Sov. Phys. JETP **32**, 866 (1971)].

[20] R. Graham, Phys. Rev. A **10**, 1762 (1974); **45**, 4198(E) (1992).

[21] For a review of work dealing with the effect of thermal noise on Rayleigh-Bénard convection see Sec. VIII D 1 of Ref. [1].

[22] R. Schmitz and E. G. D. Cohen, J. Stat. Phys. **38**, 285 (1985); **40**, 431 (1985).

[23] J. Swift and P. C. Hohenberg, Phys. Rev. A **15**, 319 (1977).

[24] P. C. Hohenberg and J. B. Swift, Phys. Rev. A **46**, 4773 (1992).

[25] M. Treiber, Phys. Rev. E **53**, 577 (1996).

[26] W. Schöpf and W. Zimmermann, Phys. Rev. E **47**, 1739 (1993).

[27] H. W. Xi, J. Viñals, and J. D. Gunton, Physica A **177**, 356 (1991); J. Viñals, H. W. Xi, and J. D. Gunton, Phys. Rev. A **46**, 918 (1992).

[28] C. W. Meyer, G. Ahlers, and D. S. Cannell, Phys. Rev. A **44**, 2514 (1991).

[29] C. W. Meyer, G. Ahlers, and D. S. Cannell, Phys. Rev. Lett. **59**, 1577 (1987).

[30] O. Osenda, C. B. Briozzo, and M. O. Cáceres, Phys. Rev. E **55**, R3824 (1997); **57**, 412 (1998).

[31] G. Ahlers, M. C. Cross, P. C. Hohenberg, and S. Safran, J. Fluid Mech. **110**, 297 (1981).

[32] H. van Beijeren and E. G. D. Cohen, Phys. Rev. Lett. **60**, 1208 (1988); J. Stat. Phys. **53**, 77 (1988).

[33] E. Bodenschatz, W. Pesch, and G. Ahlers, Annu. Rev. Fluid Mech. **32**, 709 (2000).

[34] M. A. Scherer, G. Ahlers, F. Hörner, and I. Rehberg, Phys. Rev. Lett. **85**, 3754 (2000).

[35] J. K. Platten and J. C. Legros, *Convection in Liquids* (Springer-Verlag, Berlin, 1984).

[36] S. Chandrasekhar, *Hydrodynamic and Hydromagnetic Stability* (Dover, New York, 1981).

[37] M. T. Ouazzani, J. P. Caltagirone, G. Meyer, and A. Mojtabi, Int. J. Heat Mass Transf. **32**, 261 (1989); M. T. Ouazzani, J. K. Platten, and A. Mojtabi, *ibid.* **33**, 1417 (1990); M. T. Ouazzani, J. K. Platten, H. W. Müller, and M. Lücke, *ibid.* **38**, 875 (1995).

[38] E. Schröder and K. Bühler, Int. J. Heat Mass Transf. **38**, 1249 (1995).

[39] M. Y. Chang and T. F. Lin, Phys. Rev. E **54**, 5146 (1996).

[40] X. Nicolas, A. Mojtabi, and J. K. Platten, Phys. Fluids **9**, 337 (1997).

[41] H. R. Brand, R. J. Deissler, and G. Ahlers, Phys. Rev. A **43**, 4262 (1991).

[42] H. W. Müller, M. Tveitereid, and S. Trainoff, Phys. Rev. E **48**, 263 (1993); M. Tveitereid and H. W. Müller, *ibid.* **50**, 1219 (1994).

[43] The index variables p,p' assume only the odd values 1,3,5 while the m,m' assume the even values 2,4,6 only. Other indices run through all values from 1 to 6.

[44] See, e.g., R. E. Kelly, Adv. Appl. Mech. **31**, 35 (1994) for a review, and Ref. [40] for further references.

[45] H. W. Müller, M. Lücke, and M. Kamps, Europhys. Lett. **10**, 451 (1989).